Thermal Science and Engineering 2025, 8(1), 10909.
https://doi.org/10.24294/tse10909

Article

Energy at the boundary of an elastic and thermoelastic mediums under different theories of thermoelasticity

Kamal Kumar[1], Vandana Gupta[2], Manoj Kumar[3], Shruti Goel[1,*]

[1] Department of Physical Sciences (Mathematics), Baba Mastnath University, Rohtak 124021, India
[2] Indira Gandhi National College, Behlolpur 136132, India
[3] Maharishi Markandeshwar University, Mullana 133207, India
*** Corresponding author:** Shruti Goel, shruti1922goel@gmail.com

CITATION

Kumar K, Gupta V, Kumar M, Goel S. Energy at the boundary of an elastic and thermoelastic mediums under different theories of thermoelasticity. Thermal Science and Engineering. 2025; 8(1): 10909. https://doi.org/10.24294/tse10909

ARTICLE INFO

Received: 15 December 2024
Accepted: 22 January 2025
Available online: 13 February 2025

Abstract: The study examines the impact of various theories on the reflection and transmission phenomena caused by obliquely incident longitudinal and transverse waves at the interface between a continuously elastic solid half-space and a thermoelastic half-space, using multiple thermoelastic models. Numerical calculations reveal that the thermoelastic medium supports one transmitted transverse wave and two transmitted longitudinal waves. The modulus of amplitude proportions is analyzed as a function of the angle of incidence, showing distinct variations across the studied models. Energy ratios, derived from wave amplitudes under consistent surface boundary conditions for copper, are computed and compared across angles of incidence. The results demonstrate that the total energy ratio consistently sums to one, validating energy conservation principles. Graphical comparisons of amplitude proportions and energy ratios for SV and P waves across different models illustrate significant differences in wave behavior, emphasizing the influence of thermoelastic properties on wave transmission and reflection.

Keywords: coupled model; two-phase-lag model; G-N model; three-phase-lag model; reflection; transmission; G-L model; amplitude ratio; energy ratio; L-S model

1. Introduction

The study of thermoelasticity focuses on the equilibrium of entities that are considered thermodynamic systems and whose interactions with their environment are limited to work-heat transformation, and outside forces in a given medium. In general, the deformation process itself contributes to the change in body temperature in addition to the internal and external heat sources. Under typical heat exchange conditions, the flux caused by deformation results in uneven heating. The study of thermoelasticity is the flow of heat and its effect on stress and strain when temperature and deformation field coupling take place. The elasticity and heat conduction theories are combined in the thermoelasticity hypothesis. It deals with how heat affects the deformation of an elastic medium and how deformation affects the thermal state of the medium under consideration. Numerous appealing models have been created in recent years by utilizing various theories to examine physical processes, including heat conduction and diffusion.

A study on the plane waves reflected off the surface of a thermoelastic immersed, permeable solid half-space with related surface limit conditions was provided. Using the L-S and G-N theories of generalized thermoelasticity of saturated porous medium by McCarthy [1]. The plane is the focal point of the administering conditions. Three connected longitudinal waves and a shear vertical

wave are shown to occur in a generalized thermoelastic saturated porous medium via the plane wave solution of these equations. For every incident plane wave travelling through the medium, there are reflected waves. The right possibilities for occurrence, reflected in a half-space wave present, are created using Snell's equation and meet the requisite boundary conditions. Sharma and Sidhu [2] following the derivation of the secular equation, examined the motion of plane harmonic waves in homogeneous anisotropic summed-up thermoelastic materials. Four dispersive wave modes were discovered to be feasible. The typical modes of linked thermoelasticity are three modes referred to as quasi-elastic (E). With a finite velocity of propagation, the fourth mode, alluded to as semi-warm (T) is diffusive in coupled thermoelasticity, presently looks like a wave. All the modes have been approximated at both high and low frequencies. Banerjee and Pao [3] looked into the propagation of the plane harmonic wave in unbounded anisotropic solids. Three of the four characteristic wave speeds discovered are comparable to isothermal or adiabatic elastic waves. The intensity beats, frequently known as the subsequent sound, correspond to the fourth wave, which is mostly a temperature disturbance. Numerical and graphical results are utilized to assess the velocities, slowness, and wave surfaces of the thermoelastic waves for solid helium crystals and NaF.

Puri [4] looked at plane waves in generalized thermoelasticity. In the framework of generalized thermoelasticity, the characteristics of two dilatational motions are examined. The frequency equation's precise solution is presented, and the real and imaginary wave number components precise values are computed. The behavior of the amplitude ratios for small and big frequencies is studied, along with the ranges of validity and approximate representations of this solution for large and small frequencies. Chadwick and Seet [5] published evidence for the propagation of planar harmonic body waves within a single zinc crystal. Dhaliwal and Sherief [6] expanded the generalized thermoelasticity theory for anisotropic heat-conducting thermoelastic materials. In a thermoelastic half-space, wave propagation was studied by Chandrasekharaiah [7]. The motion of summed-up thermoelastic waves transversed in an isotropic medium was covered by Singh and Sharma [8]. Sharma [9] discovered a connection between the concepts of thermoelasticity and poroelasticity and developed a math-related model for the wave motion in an anisotropic generalized medium of thermoelasticity. It was investigated how inhomogeneous waves propagate in anisotropic piezo-thermoelastic mediums.

Prasad et al. [10] described the movement of planar harmonic waves under thermoelasticity with double-stage slack. Asymptotic expressions of several wave field characterizations, for example, explicit loss, phase speed, adequacy ratios, and penetration profundity, result for both low and high values of frequency. Analytical techniques are used to determine the precise dispersion relations for plane waves. Using the computer tool Mathematica, the mathematical upsides of particular wave fields at moderate frequencies are found. The results are then shown in a number of images to illustrate the analytical findings.

Three-dimensional thermoelastic wave movements under the influence of a buried source were shown in half-space by Lykotrafitis et al. [11]. The propagation of waves in a generic anisotropic poroelastic medium was explored by Sharma [12]. Venkatesan and Ponnusamy [13] depicted the wave engendering in a summed-up

thermoelastic strong chamber under different circumstances. Kumar and Kansal [14] were examined transversely isotropic thermoelastic diffusive plates by for the motion of a wave that is called lamb. Yu et al. [15] directed thermoelastic wave proliferation in stacked plates was displayed without energy misfortune. Kumar and Gupta [16] described the reflection and transmission of plane waves at the boundary between a flexible half-space and a portion of a thermoelastic half-space. Youssef and El-Bary [17] studied the theory of hyperbolic two-temperature generalized thermoelasticity. Lata et al. [18] worked on transversely isotropic magneto-thermoelastic rotating materials in the Lord-Shulman model and the thermomechanical interactions resulting from time-harmonic sources. Kumar et al. [19] studied wave interference, by considering the fractional order derivative condition on an elastic and two-temperature generalized thermoelastic half-space. Sherief et al. [20] examined how semiconductor elastic materials behaved when exposed to an external magnetic field. The framework takes into account how thermal, elastic, and plasma waves interact. The thermoelastic behavior of semiconductor materials in plasma is described by a new completely coupled mathematical model. Ding et al. [21] studied nonlocal elasticity captures these microstructural interactions, which are crucial for interpreting the overall behavior of the composite. The mechanical response at each position in the examined composite materials with heterogeneous microstructures is influenced by surrounding inclusions or fibers. Li et al. [22] worked on influence of time-dependent effects and long-range forces on the mechanical behavior of nanoscale objects, such as thin films, nanotubes, and nanowires is well captured by this model. Biological tissues, particularly in polymers and soft materials, where the response to loading varies on both time and previous deformations, the model describes history-dependent behavior for viscoelastic materials that is essential for comprehending stress relaxation and creep. Kumar [23] examined micropolar elasticity is appropriate for capturing the varying rotations and deformations of the fibers and matrix in fiber-reinforced composites. The theory also applies to porous and granular materials, such as powders or soils, where complicated mechanical behavior can result from the rotation of individual grains relative to one another. Furthermore, because classical elasticity is unable to explain the behavior of high-frequency, short-wavelength waves, such as ultrasonic waves, in microstructured materials, micropolar elasticity is essential for comprehending high-frequency wave propagation. Yadav et al. [24] examined the nonlocal elasticity reflection phenomena in a hygrothermal medium. Three integrated plane waves—longitudinal displacement, shear vertical SV wave propagation in the medium, moisture diffusion mD-wave, and thermal diffusion TD-wave—are predicted by the plane wave solution. The hygrothermal medium's P, mD, TD, and SV wave velocities are calculated. For the incidence of a hygrothermal plane wave, expressions for the energy ratio and reflection coefficient are created and shown graphically. Abd-Alla et al. [25] studied the wave motion under the effect of a magnetic field in a vacuum and compared the dual-phase-lag model and Lord-Shulman theory in the absence and presence of a magnetic field. Othman et al. [26] compared the reflection of generalized thermoelastic waves for the different theories (CT, L-S, G-L) in the presence of rotation, magnetic field, initial stress and the two-temperature parameter.

The interesting phenomena at a plane point of interaction between a versatile solid half-space and on the other side of the plane, considering different models are discussed in the current work. Work has been done on different theories given by authors, such as couple theory, Lord and Shulman (L-S) theory, Green and Naghdi (G-N) theory, Green and Lindsay (G-L) theory, and two-phase-lag and three-phase-lag theories of thermoelastic solids in other half-space. The amplitude proportions of various refracted and reflected waves to the wave that approaches the boundary are determined. The expressions of the energy proportions for the incident wave to the different reflected waves along with the refracted waves are further found using the amplitude ratios. These energy ratios are visually shown and comparisons are provided for several ideas. The values of energy ratio can be negative or positive but the overall sum of all energies is the same in both cases. Thus, the total sum of energies in every theory is one. Because of the values being both negative and positive, they affect each other and have a sum of 1 for each incident angle. So, during the interaction, the rule of conservation of energy is confirmed.

2. Governing equations

The equation for thermal conductivity, which incorporates the dilatation term based on the thermodynamics of irreversible processes, was satisfactorily derived by Biot [27]. To resolve the contradiction in the conventional uncoupled theory, which states that elastic changes have no impact on temperature, he developed the idea of coupled thermoelasticity. The coupled theory of thermoelasticity results from the coupling of the temperature and strain fields. Equation of motion given as:

$$(\lambda + \mu)v_{k,ki} + \mu v_{i,kk} - \gamma T_{,i} + \rho F_i = \rho \ddot{v}_i \tag{1}$$

Coupled theory equation of heat conduction is:

$$KT_{,ii} + Q = \rho c\dot{T} + \gamma T_0 \dot{e}_{kk} \tag{2}$$

By modifying the law of heat conduction, Lord and Shulman [28] introduced the theory of generalized thermoelasticity with one relaxation time (the isotropic body), which resolves the paradox of infinite speeds of heat and elastic disturbance propagation present in both the coupled and uncoupled theories of thermoelasticity. The theory of heat conduction is as follows:

$$KT_{,ii} = \left(1 + \tau_0 \frac{\partial}{\partial t}\right)\left(\rho c\dot{T} + \gamma T_0 \dot{e}_{kk} - Q\right) \tag{3}$$

The theory of thermoelasticity with two relaxation times or the theory of temperature-rate-dependent thermoelasticity, as presented by Green and Lindsay [29], is a further generalization of the coupled theory of thermoelasticity and is as follows:

The equation of motion and the equation of heat conduction are respectively:

$$(\lambda + \mu)v_{k,ki} + \mu v_{i,kk} - \gamma\left(T + \tau_1 \dot{T}\right)_{,i} + \rho F_i = \rho \ddot{v}_i \tag{4}$$

$$KT_{,ii} + Q = \rho c\left(\dot{T} + \tau_0 \ddot{T}\right) + \gamma T_0 \dot{e}_{kk} \tag{5}$$

For homogeneous and isotropic materials, Green and Naghdi [30,31] suggested three thermoelasticity models. The terms type-I, type-II, and type-III thermoelasticity are used to refer to the three different theories. While the second and third models provide for additional sound effects, the first of these models is identical with coupled thermoelasticity. The Green-Naghdi (Type-III) theory of the heat conduction equation is:

$$\mathrm{KT}_{,ii}+\mathrm{K}^{*}v_{,ii}+\rho\dot{r}=\rho c\ddot{\mathrm{T}}+\gamma T_0\ddot{e}_{kk} \tag{6}$$

RoyChoudhuri [32] identified the initiative in the three-phase-lag model heat transport equation as:

$$\left(1+\tau_q\frac{\partial}{\partial t}\right)\left(\rho c\dot{T}+\gamma T_0\dot{e}_{kk}-Q\right)=\tau_v^{*}T_{,ii}+K\tau_T\dot{T}_{,ii}+K^{*}v_{,ii} \tag{7}$$

We assume that the material parameters satisfy the inequality $0\le\tau_v<\tau_t<\tau_q$. Then the equation states that the temperature gradient and the thermal displacement gradient established across a material volume located at position $P(r)$ at time $t+\tau_t$ and $t+\tau_v$ result in heat flux to flow at a different instant of time τ_q. The third delay time τ_v may be interpreted as the phase lag of the thermal displacement gradient.

Tzou [33] defined the two-phase-lag model heat conduction equation as:

$$K\left(1+\tau_T\frac{\partial}{\partial t}\right)T_{,ii}=\left(1+\tau_q\frac{\partial}{\partial t}+\frac{1}{2}\tau_q^2\frac{\partial^2}{\partial t^2}\right)\left(\rho\mathrm{c}\dot{\mathrm{T}}+\gamma T_0\dot{e}_{kk}-Q\right) \tag{8}$$

According to which the temperature gradient at a point P at time $t+\tau_t$ corresponds to the heat flux vector at P at time $t+\tau_q$. The delay time τ_t is interpreted as that caused by the microstructural interactions, such as photon-electron interaction or photon scattering, and is called the phase lag of the temperature gradient. The other delay time τ_q is interpreted as the thermal relaxation time due to the fast transient effect of thermal inertia and is called the phase lag of the heat flux. Without even a trace of an outer intensity source (body forces and heat sources), a minimized type of situation for the displacement and temperature field for the thermoelasticity theories previously described in Equations (1)–(8) is as follows.

The equations of motion:

$$(\lambda+\mu)v_{k,ki}+\mu v_{i,kk}-\gamma\left(1+\tau_1\frac{\partial}{\partial t}\right)T_{,i}=\rho\ddot{v}_i \tag{9}$$

The heat conduction equation:

$$\begin{aligned}&K'\left(n^{*}+t_1\frac{\partial}{\partial t}+t_3\frac{\partial^2}{\partial t^2}\right)T_{,ii}=\\&\rho c\left(n_1\frac{\partial}{\partial t}+\tau_0\frac{\partial^2}{\partial t^2}+t_2\frac{\partial^3}{\partial t^3}+t_4\frac{\partial^4}{\partial t^4}\right)T+T_0\gamma\left(n_1\frac{\partial}{\partial t}+n_0\tau_0\frac{\partial^2}{\partial t^2}+t_2\frac{\partial^3}{\partial t^3}+t_4\frac{\partial^4}{\partial t^4}\right)e_{kk}\end{aligned} \tag{10}$$

where $n^{*},t_1,t_3,n_1,\tau_0,t_2,t_4,n_0$ are parameters. Which are defined below for each case.

The Equations (9) and (10) are reduced to several special cases as follows:

Case 1: Coupled theory condition of thermoelasticity is obtained.

$$n^* = 1, t_1 = 0, n_1 = 1, t_2 = 0, t_3 = 0, \tau_0 = 0, t_4 = 0, \tau_1 = 0.$$

Case 2: The L-S theory of thermoelasticity holds.

$$n^* = 1, n_1 = 1, t_1 = 0, t_2 = 0, \tau_1 = 0, t_3 = 0, n_0 = 1, t_4 = 0, \tau_0 = 0.$$

Case 3: The G-L theory of thermoelasticity follows.

$$n^* = 1, t_1 = 0, n_0 = 0, t_2 = 0, \tau_0 = 1, t_3 = 0, n_1 = 1, t_4 = 0, \tau_1 \geq \tau_0.$$

Case 4: The G-N (Type-III) theory of thermoelasticity is obtained when.

$$n^* > 0, n_1 = 0, t_1 = 1, t_2 = 0, \tau_0 = 1, t_3 = 0, t_4 = 0, n_0 = 1.$$

Case 5: The Three-phase-lag theory of thermoelasticity is obtained when.

$$\tau_0 = 1, n_0 = 1, n_1 = 0, \tau_1 = 0, t_2 = \tau_q, t_1 = 1 + n^* \tau_v, t_3 = \tau_T, t_4 = \frac{\tau_q^2}{2}.$$

Case 6: The Two-phase-lag theory of thermoelasticity is as follows:

$$n^* = 1, \tau_0 = \tau_q,\ n_0 = 1, n_1 = 1, \tau_1 = 0, t_1 = \tau_T,\ t_2 = \frac{\tau_q^2}{2}, t_3 = 0,\ t_4 = 0.$$

The temperature-stress-strain relationship is denoted as follows:

$$\sigma_{ij} = 2\mu e_{ij} + \lambda e_{kk}\delta_{ij} - \gamma\left(1 + \tau_1 \frac{\partial}{\partial t}\right) T\delta_{ij} \tag{11}$$

The strain is related to displacement as follows:

$$e_{ij} = \frac{1}{2}\left(v_{i,j} + v_{j,i}\right) \tag{12}$$

where

$T = \theta - T_0$, increase in temperature. T_0, temperature of reference for the object chosen to hold $\left|\frac{T}{T_0}\right| << 1$. θ, temperature which is considered absolute for medium. C_E, specific heat when strain is constant. ρ, represents the density, which is not dependent on time. σ_{ij}, are the stress components. e_{ij}, strain components. e_{kk}, represents dilatation. v, is the thermal displacement. τ_q, heat flux from phase lag. τ_T, temperature of phase lag. K^*, is the material characteristic. τ_v, thermal displacement of phase lag. K', coefficient of thermal conductivity. $\gamma = (3\lambda + 2\mu)\alpha_t$; μ, λ are the Lame's constants, α_t is the term used as a thermal linear expansion term. v_i, components in the plane of the displacement vector v.

3. Discussion of problem

We assume a homogeneous isotropic space with an interface along $x_3 = 0$ containing thermoelastic theories in $x_3 > 0$ (Medium II) with x_3 points vertically upward and an isotropic elastic solid in $x_3 < 0$ (Medium I) with x_3 points vertically downward. (x_1, x_2, x_3) to be a coordinate of the Cartesian plane. The wave front of the reflection and transmission issue being studied here is parallel to the x_3 axis and is in the two-dimensional plane $x_1 - x_3$ shown in (**Figure 1**). Let's assume that an incident plane harmonic wave P or SV, travels inside the isotropic upper half-elastic solid space.

To solve the problem related to two-dimensional space, consider the displacement vector in medium II as:

$$v_i = (v_1, 0, v_3) \tag{13}$$

Here, dimensionless quantities are defined as:

$$\begin{aligned} x_i^{'} &= C_0\eta x_i, v_i^{'} = C_0\eta v_i, v^{'e}_i = C_0\eta {v_i}^e, i = 1,3, \\ t^{'} &= {C_0}^2\eta t, \tau_1^{'} = {C_0}^2\eta\tau_1, T^{'} = \frac{T}{T_0}, \\ \sigma_{ij}^{'} &= \frac{\sigma_{ij}}{\rho C_0^2}, \sigma_{ij}^{'e} = \frac{{\sigma_{ij}}^e}{\rho C_0^2}, P^{*e'} = \rho C_0 P^{*e}, P_{ij}^{*'} = \rho C_0 P_{ij}^{*}, i,j = 1,3 \end{aligned} \tag{14}$$

where

$${C_0}^2 = \frac{\lambda+2\mu}{\rho}, \eta = \frac{\rho C_E}{K}.$$

By using the Equations (13) and (14) in Equations (9) and (10), after suppressing the primes, the resulting Equations are (15)–(17) as follows:

$$(\beta^2 - 1)\frac{\partial}{\partial x_1}\left(\frac{\partial v_1}{\partial x_1} + \frac{\partial v_3}{\partial x_3}\right) + \nabla^2 v_1 - b\left(1 + \tau_1\beta^2 a\frac{\partial}{\partial t}\right)\left(\frac{\partial T}{\partial x_1}\right) = \beta^2\frac{\partial^2 v_1}{\partial t^2} \tag{15}$$

$$(\beta^2 - 1)\frac{\partial}{\partial x_3}\left(\frac{\partial v_1}{\partial x_1} + \frac{\partial v_3}{\partial x_3}\right) + \nabla^2 v_3 - b\left(1 + \tau_1\beta^2 a\frac{\partial}{\partial t}\right)\left(\frac{\partial T}{\partial x_3}\right) = \beta^2\frac{\partial^2 v_3}{\partial t^2} \tag{16}$$

$$\begin{aligned} &\left(n^* + t_1 c\frac{\partial}{\partial t} + t_3 c^2\frac{\partial^2}{\partial t^2}\right)\nabla^2 T = \\ &\left(n_1\frac{\partial}{\partial t} + \tau_0 c\frac{\partial^2}{\partial t^2} + t_2 c^2\frac{\partial^3}{\partial t^3} + t_4 c^3\frac{\partial^4}{\partial t^4}\right)T + \in\left(n_1\frac{\partial}{\partial t} + n_0\tau_0 c\frac{\partial^2}{\partial t^2} + t_2 c^2\frac{\partial^3}{\partial t^3} + t_4 c^3\frac{\partial^4}{\partial t^4}\right)\left(\frac{\partial v_1}{\partial x_1} + \frac{\partial v_3}{\partial x_3}\right) \end{aligned} \tag{17}$$

where

$$\in = \frac{\gamma}{\rho C_E}, \beta^2 = \frac{\lambda + 2\mu}{\mu}, b = \frac{\gamma T_0}{\mu}, a = \frac{\mu\eta}{\rho}, c = C_0^2\eta \tag{18}$$

The potential operates as follows in relation to the non-dimensional displacement components v_1, v_3 in Medium II.

$$v_1 = \frac{\partial\phi}{\partial x_1} - \frac{\partial\psi}{\partial x_3}, v_3 = \frac{\partial\phi}{\partial x_3} + \frac{\partial\psi}{\partial x_1} \tag{19}$$

where ψ notation is used for the potential transverse waves, φ notation is used for the potential longitudinal waves. Substituting Equation (19) in the Equations (15)–(17) results in the following equations:

$$\beta^2\left(\nabla^2 - \frac{\partial^2}{\partial t^2}\right)\varphi - b\left(1 + \tau_1\beta^2 a\frac{\partial}{\partial t}\right)T = 0 \tag{20}$$

$$\nabla^2\Psi - \beta^2\frac{\partial^2\Psi}{\partial t^2} = 0 \tag{21}$$

$$\left(n^* + t_1 c\frac{\partial}{\partial t} + t_3 c^2\frac{\partial^2}{\partial t^2}\right)\nabla^2 T = \left(n_1\frac{\partial}{\partial t} + \tau_0 c\frac{\partial^2}{\partial t^2} + t_2 c^2\frac{\partial^3}{\partial t^3} + t_4 c^3\frac{\partial^4}{\partial t^4}\right)T + \in\left(n_1\frac{\partial}{\partial t} + n_0\tau_0 c\frac{\partial^2}{\partial t^2} + t_2 c^2\frac{\partial^3}{\partial t^3} + t_4 c^3\frac{\partial^4}{\partial t^4}\right)\nabla^2\varphi \tag{22}$$

For propagation of harmonic waves in the considered plane as:

$$\{\phi, \psi, T\}(x_1, x_3, t) = \{\bar{\phi}, \bar{\psi}, \bar{T}\}e^{-i\omega t} \tag{23}$$

Here the particle's angular frequency of vibration is ω. After simplifying the Equations (20) and (22) by substituting Equation (23), we obtained Equation (24):

$$[R\nabla^4 + S\nabla^2 + T]\bar{\phi} = 0 \tag{24}$$

where

$R = \beta^2(n^* - it_1 c\omega - t_3 c^2\omega^2)$,
$S = \beta^2(in_1\omega + \tau_0 c\omega^2 + it_2 c^2\omega^3 - t_4 c^3\omega^4) + b \in (1 - i\tau_1\beta^2 a\omega)(in_1\omega + \tau_0 n_0 c\omega^2 + it_2 c^2\omega^3 - t_4 c^3\omega^4)$,
$T = \beta^2\omega^2(n^* - i(t_1 c - n_1)\omega - (t_3 - it_2)c^2\omega^2 + \tau_0 c\omega^2 - t_4 c^3\omega^4)$.

The general form of Equation (24) solution can be considered as:

$$\bar{\phi} = \bar{\phi}_1 + \bar{\phi}_2 \tag{25}$$

Taking $i = 1, 2$ the potentials satisfy the equations of wave, resulting in:

$$\left[\nabla^2 + \frac{\omega^2}{V_i^2}\right]\bar{\phi}_i = 0 \tag{26}$$

Characteristic equations whose roots are named V_1, V_2 for the P and T waves respectively, are given below:

$$TV^4 - S\omega^2 V^2 + R\omega^4 = 0 \tag{27}$$

With the help of Equations (21) and (23), we get:

$$\left[\nabla^2 + \frac{\omega^2}{V_3^2}\right]\bar{\psi} = 0 \tag{28}$$

where $V_3 = \frac{1}{\beta}$, velocity of a transverse wave (SV wave) in medium $x_3 > 0$.

Using Equations (22), (23), (25) and (26), we obtain:

$$\{\varphi, T\} = \sum_{i=1}^{2}\{1, m_i\}\varphi_i \tag{29}$$

where

$$m_i = \frac{(in_1\omega + \tau_0 n_0 c\omega^2 + it_2 c^2\omega^3 - t_4 c^3\omega^4) \in \omega^2}{V_i^2[(n^* - it_1 c\omega - t_3 c^2\omega^2)\nabla^2 + (in_1\omega + \tau_0 c\omega^2 + it_2 c^2\omega^3 - t_4 c^3\omega^4)]}, i = 1, 2 \tag{30}$$

The fundamental equation for homogeneous isotropic elastic solids is expressed as:

$$(\lambda^e + \mu^e)\nabla(\nabla v_i{}^e) + \mu\nabla^2 v_i{}^e = \rho^e\ddot{v}_i \tag{31}$$

where μ^e, λ^e are Lame's constants. v_i^e, represents the components in a Cartesian plane having a displacement vector v^e. ρ^e, indicates the density in the medium $x_3 < 0$.

$$e_1^e = \frac{\partial v_1^e}{\partial x_1} + \frac{\partial v_3^e}{\partial x_3}.$$

For a two-dimensional plane $x_1 - x_3$ problem, the components $v_i^e = (v_1^e, 0, v_3^e)$ can be considered as:

$$v_1^e = \frac{\partial \phi^e}{\partial x_1} - \frac{\partial \psi^e}{\partial x_3}, v_3^e = \frac{\partial \phi^e}{\partial x_3} + \frac{\partial \psi^e}{\partial x_1} \tag{32}$$

where potential φ^e corresponds to longitudinal wave and ψ^e corresponds to transversal wave equations from using Equations (31) and (32):

$$\nabla^2 \varphi^e = \frac{1}{\alpha_p^{2e}} \ddot{\varphi}^e \tag{33}$$

$$\nabla^2 \psi^e = \frac{1}{\beta_s^{2e}} \ddot{\psi}^e \tag{34}$$

where

$$\alpha_p^e = \sqrt{\frac{(\lambda^e + 2\mu^e)}{\rho^e}}, \beta_s^e = \sqrt{\frac{\mu^e}{\rho^e}}, \ \alpha = \frac{\alpha_p^e}{C_0}, \ \beta = \frac{\beta_s^e}{C_0} \tag{35}$$

The isotropic elastic medium's stress tensor and strain tensor are respectively given by:

$$\begin{aligned} \sigma_{ij}^e &= 2\mu^e e_{ij}^e + \lambda^e e_{kk}^e \delta_{ij} \\ e_{ij}^e &= \frac{1}{2}\left(v_{i,j}^e + v_{j,i}^e\right) \end{aligned} \tag{36}$$

where e_{ii}^e is the dilatation.

4. Wave potential functions

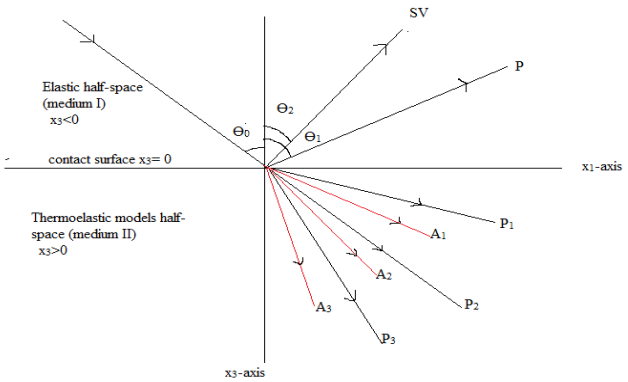

Figure 1. Geometry of the problem.

Consider a harmonic wave (P or SV) striking at the interface $x_3 = 0$ and travelling in medium $x_3 < 0$ and $x_3 > 0$ (**Figure 1**) shown.

In medium $x_3 > 0$, the potential functions satisfying Equations (34) and (33) can be taken as Kumar and Kansal [34]:

$$\phi^e = A_0^{'e}\exp\left[i\omega\left\{\left((x_1\sin\theta_0 + x_3\cos\theta_0)/\alpha\right) - t\right\}\right] + A_1^{'e}\exp\left[i\omega\left\{\left((x_1\sin\theta_1 - x_3\cos\theta_1)/\alpha\right) - t\right\}\right] \quad (37)$$

$$\psi^e = B_0^{'e}\exp\left[i\omega\left\{\left((x_1\sin\theta_0 + x_3\cos\theta_0)/\beta\right) - t\right\}\right] + B_1^{'e}\exp\left[i\omega\left\{\left((x_1\sin\theta_2 - x_3\cos\theta_2)/\beta\right) - t\right\}\right] \quad (38)$$

ω is the angular frequency, and the coefficients $A_0^{'e}$, $B_0^{'e}$, $A_1^{'e}$ and $B_1^{'e}$ are the amplitudes of the incident P (or SV), reflected P and reflected SV waves respectively.

Following Borcherdt [35], the complete structure of the refracted wave's wave field in isotropic thermoelastic solid half-space may be expressed as:

$$\{\phi, T\} = \sum_{i=1}^{2}\{1, m_i\}B_i^{'}\, exp\left(A_i^{'}.r\right)exp\{i(P_i.r - \omega t)\} \quad (39)$$

$$\psi = B_3^{'}exp\left(A_3^{'}.r\right)exp\{i(P_3.r - \omega t)\} \quad (40)$$

where the coupling constants m_i, $i = 1, 2$ are given in the above Equation (30). $B_i^{'}, i = 1, 2, 3$ be the coefficients taken to represent the amplitudes of refracted P, T and SV waves respectively. The wave motion vector considered $P_i, i = 1, 2, 3$ as well as the attenuation factor $A_i^{'}, i = 1,\ 2,\ 3$ are given by:

$$P_i = \xi_R\hat{x}_1 + dV_{iR}\hat{x}_3,\ \mathrm{A}_i^{'} = -\xi_{\mathrm{I}}\hat{x}_1 - dV_{iI}\hat{x}_3,\ i = 1, 2, 3 \quad (41)$$

where

$$dV_i = dV_{iR} + idV_{iI} = p.v.\left(\frac{\omega^2}{V_i^{\,2}} - \xi^2\right),\ i = 1, 2 \quad (42)$$

where $\hat{x}_1, \hat{x}_3$ denote the unit vector in the x_1 and x_3 directions, respectively, where p.v. stands for the primary value of the complex quantity generated from the square root. $\xi = \xi_R + i\xi_{\mathrm{I}}$, where ξ represents the wave number, which is in the form of a complex number, R and I stand for complex numbers having the real and imaginary parts correspondingly. Consider $\xi_R \geq 0$. In the isotropic thermoelastic medium, different models are given by complex numbers:

$$\xi = -i\left|A_i^{'}\right| sin\left(\theta_i^{'} - \gamma_i^{'}\right) + |P_i|\, sin\,\theta_i^{'},\ i = 1, 2, 3 \quad (43)$$

where $\theta_i^{'}$ indicates the refracted angle in Medium II and the angle between the wave propagates and the attenuation vector is taken as $\gamma_i^{'}$. If $\left|A_i^{'}\right| \neq 0$, then $\theta_i^{'} = \gamma_i^{'}$, $i =$ 1,2,3, implies that three refracted waves are in the direction of x_3 axis.

5. Surface boundary conditions

The surface boundary conditions with the partition that must be fulfilled $x_3 = 0$ are as follows:

a) Mechanical conditions:

$$\sigma_{33}{}^{e} = \sigma_{33} \quad (44)$$

$$\sigma_{31}{}^{e} = \sigma_{31} \tag{45}$$

b) Displacement conditions:

$$v_1{}^{e} = v_1 \tag{46}$$

$$v_3{}^{e} = v_3 \tag{47}$$

c) Thermal conditions:

$$\frac{\partial T}{\partial x_3} + hT = 0 \tag{48}$$

where

h indicates the coefficient of heat transfer.

$h \to 0$ is equivalent to a boundary with insulation.

$h \to \infty$ corresponding to a boundary that is isothermal.

$$\begin{matrix} \sigma_{31} = \frac{\mu(v_{1,3}+v_{3,1})}{\rho C_0^2}, \sigma_{33} = \frac{[(\lambda^e+2\mu^e)v_{3,3}^e+\lambda^e v_{1,1}^e]}{\rho C_0^2}, \\ \sigma_{31}^e = \frac{\mu^e(v_{1,3}^e+v_{3,1}^e)}{\rho C_0^2}, \sigma_{33}^e = \frac{[(\lambda^e+2\mu^e)v_{3,3}^e+\lambda^e v_{1,1}^e]}{\rho C_0^2} \end{matrix}.$$

Here, construct a system of five equations of non-homogeneous nature in six unknowns by including the potentials provided by Equations (37)–(40) into the earlier boundary conditions Equations (44)–(48).

$$\sum_{k=1}^{5} c_{ik} Z_k = g_i \tag{49}$$

In addition to Snell's law provided by:

$$\xi_R = \frac{\omega \sin\theta_0}{V_0} = \frac{\omega \sin\theta_1}{\alpha} = \frac{\omega \sin\theta_2}{\beta} \tag{50}$$

where $Z_k = |Z_k|e^{i\psi_k^*}$, $|Z_k|$, ψ_k^*, $k = 1, 2, 3, 4, 5$ represents the proportion (ratios) of amplitudes and phase shifts of refracted P, refracted T, refracted SV, reflected P and reflected SV waves with respect to incident waves, c_{ik}, $(i, k = 1, 2, 3, 4, 5)$. Refer to Appendix A.

Also,

$$V_0 = \begin{cases} \alpha, \text{incident P-wave} \\ \beta, \text{incident SV-wave} \end{cases} \tag{51}$$

And,

$$\xi_I = 0.$$

Therefore, in x_3-direction waves are attenuated. The coefficients g_i, $i = 1, 2, 3, 4, 5$ for the right side of the Equation (49) can be written as:

$$\begin{matrix} g_i = \begin{cases} (-1)^{i+1} c_{i2}, \text{incident SV wave} \\ (-1)^{i} c_{i1}, \text{incident P wave} \end{cases} ; i = 1 \cdots 4, \\ g_i = 0 \qquad\qquad\qquad\qquad\qquad ; i = 5 \end{matrix} \tag{52}$$

According to Achenbach [36], now let's take a look at a unit-sized surface element that sits at the intersection of two media and calculate the amount of energy distributed.

$$P^* = \sigma_{lm} l_m \dot{v}_l \tag{53}$$

The stress tensor is denoted by σ_{lm} and v_i is the component of the particle displacement, I_m the unit normal vector is in the form of a direction cosine, and $\hat{I}$ the normal outward vector is considered part of the area element. Over a period, the time average is denoted by $\langle P^* \rangle$.

6. Energy partition

Physically, it is necessary to take into account how the incident wave's energy is distributed among the numerous refracted and reflected waves at the planar contact. According to Achenbach [36], the pace of energy movement per unit region is as follows:

$$\begin{cases} \langle P^{*e} \rangle = \text{Real}\langle\sigma\rangle_{13}^{e} \text{Real}\langle\dot{v}_1^{e}\rangle + \text{Real}\langle\sigma\rangle_{33}^{e} \text{Real}\langle\dot{v}_3^{e}\rangle (\text{elastic solid medium}) \\ \langle P_{ij}^{*} \rangle = \text{Real}\langle\sigma\rangle_{13}^{(i)} \text{Real}\left\langle\dot{v}_1^{(j)}\right\rangle + \text{Real}\langle\sigma\rangle_{33}^{(i)} \text{Real}\left\langle\dot{v}_3^{(j)}\right\rangle (\text{thermoelastic solid medium}) \end{cases} \tag{54}$$

By Achenbach [29], consider two complex functions m and n, and we have:

$$\langle \text{Re a l(m)} \rangle \langle \text{Re a l(n)} \rangle = \frac{1}{2} \langle \text{Re a l(m}\bar{\text{n}}\text{)} \rangle \tag{55}$$

The energy ratio E_i used for the reflected SV-waves and reflected P-waves is (Kumar and Kansal [34]):

$$E_i = -\frac{\langle P_i^{*e} \rangle}{\langle P_0^{*e} \rangle}, i = 1,2 \tag{56}$$

$$E_{ij} = \frac{\langle P_{ij}^{*} \rangle}{\langle P_0^{*e} \rangle}, i,j = 1,\ 2,\ 3 \tag{57}$$

where E_2, E_1 are the reflected SV and P waves energy ratios respectively. The leading diagonal represents the energy matrix E_{ij} in Equation (57). On the other hand, it represents the P, T and SV waves energy ratios, while the sum of the elements other than the diagonal entries provides the interaction energy share for all refracted waves in Medium-II.

$$E_{RR} = \sum_{i=1}^{3} \left(\sum_{j=1}^{3} E_{ij} - E_{ii} \right) \tag{58}$$

And,

$$\langle P_1^{*e} \rangle = \frac{1}{2} \frac{\omega^4 \rho^e c_0^2}{\alpha} \left| A'^{e}_1 \right|^2 \text{Re}(\cos\theta_1), \langle P_2^{*e} \rangle = \frac{1}{2} \frac{\omega^4 \rho^e c_0^2}{\beta} \left| B'^{e}_1 \right|^2 \text{Re}(\cos\theta_2).$$

$$\langle P_0^{*e}\rangle = \begin{cases} \langle P_0^{*e}\rangle = -\frac{1}{2}\frac{\omega^4\rho^e c_0^2}{\alpha}\left|A'^{e}_{0}\right|\cos\theta_0, (\text{ incident P}-\text{wave}) \\ \langle P_0^{*e}\rangle = -\frac{1}{2}\frac{\omega^4\rho^e c_0^2}{\beta}\left|B'^{e}_{0}\right|\cos\theta_0, (\text{incident } SV-\text{wave}) \end{cases} \quad (59)$$

$\langle P_{ij}^{*}\rangle$,; i ∈ {1,2,3}, j ∈ {1,2,3}. Refer to Appendix B.

Through the relationship, it is possible to see the incident energy holds the conservation of energy throughout the process for all studied theories.

$$E_{11} + E_{22} + E_{33} + E_1 + E_2 + E_{RR} = 1 \quad (60)$$

7. Numerical results and discussion

Here are some numerical findings for the copper substance (Sherief and Saleh [37]), for which the following physical information is provided:

$C_E = 383.1 JKg^{-1}K^{-1},\ K = 0.383\times10^{3} Wm^{-1}K^{-1}, T_0 = 0293K, h = 0, \alpha_t = 1.78\times10^{-5}K^{-1},$
$\lambda = 7.76\times10^{10} Kgm^{-1}s^{-2}, \rho = 8.954\times10^{3} Kgm^{-3}, \mu = 3.86\times10^{10} Kgm^{-1}s^{-2}.$

Bullen [38] provides the numerical values for granite in an elastic medium.

$\alpha^e = 5.27\times10^{3} ms^{-1}, \rho^e = 2.65\times10^{3} Kgm^{-3},\ \beta^e = 3.17\times10^{3} ms^{-1}.$

By considered Cases 1 to 6 defined above. In particular, for G-L theory consider $\tau_0 = 1$, $\tau_1 = 2$, for G-N theory consider $n^* = 2$. The values of energy ratios and an energy matrix defined in the previous section have been calculated using the software MATLAB R2023a for various values of initial falling angle $\theta°$ in interval 0° to 90° and the frequency $\omega = 200\pi$ Hz used for incident P and SV waves. The effect of changes in incident angle with the energy ratios for coupled theory, L-S theory, G-N theory, G-L theory, three-phase-lag theory, and two-phase-lag theory has been shown in **Figures 2–7** (for P wave) and effect of angle on amplitude is observed in **Figures 8–12** (for P) respectively. The effect of angle on energy ratio is observed in **Figures 13–18** (for SV waves) and effect of angle on amplitude is observed in **Figures 19–23** (for SV waves) respectively. In all plotted graph, black, red, blue, pink, green, and navy-blue rectangular strips represent coupled models, the L-S model, the G-L model, the G-N model, the three-phase-lag theory and the two-phase lag theory respectively. 3D graphs are generated to demonstrate the impact of various thermoelasticity theories.

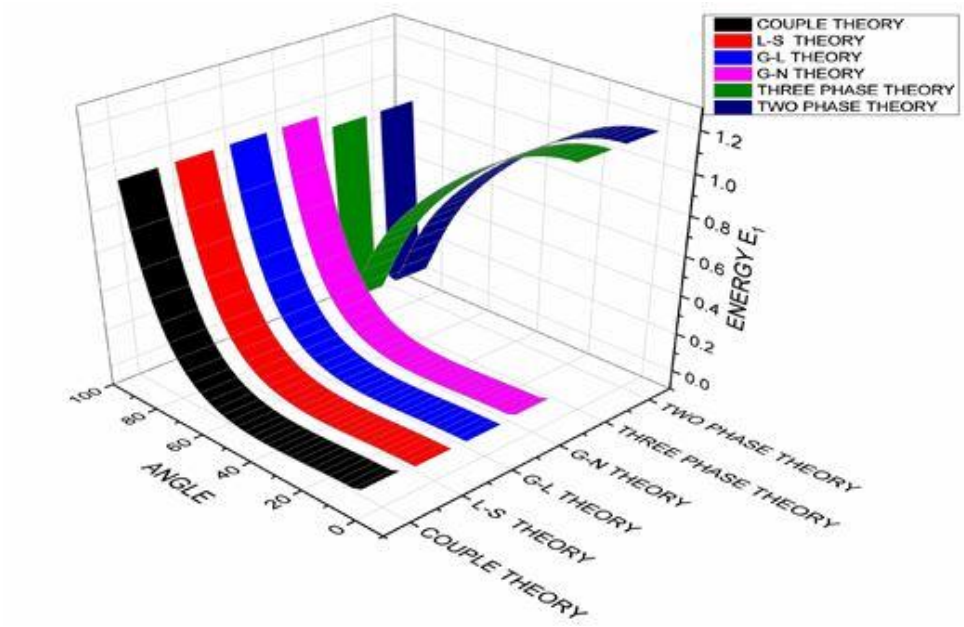

Figure 2. Changes in energy ratio E_1 w.r.t angle for $\theta°$ P wave.

It is observed in **Figure 2** that Coupled, L-S, G-L and G-N model energies show the same behavior the values of energy proportion E_1 increase with the increase in value of angle incidence $0° \leq \theta° \leq 90°$, and three-phase-lag model analysis and two-phase-lag model analysis show the same behavior in which the value of energy decreases as $\theta°$ increases and increases continuously at $\theta° = 86°$.

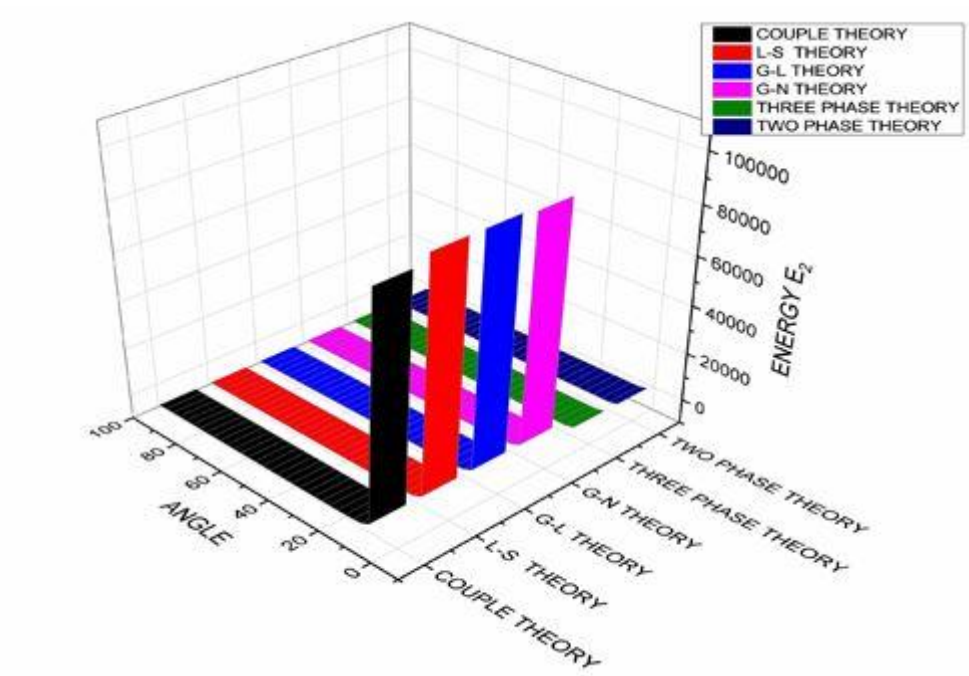

Figure 3. Changes in energy ratio E_2 w.r.t angle $\theta°$ for P wave.

Further, **Figure 3** shows that the values of E_2 decrease as $\theta°$ is in the range $10° \leq \theta° \leq 20°$ and thereafter remain constant as the value of $\theta°$ increases continuously for the Coupled L-S, G-L and G-N models. Three- and two-phase-lag models appear to be constant as their values are above 0 but very small compared to other models.

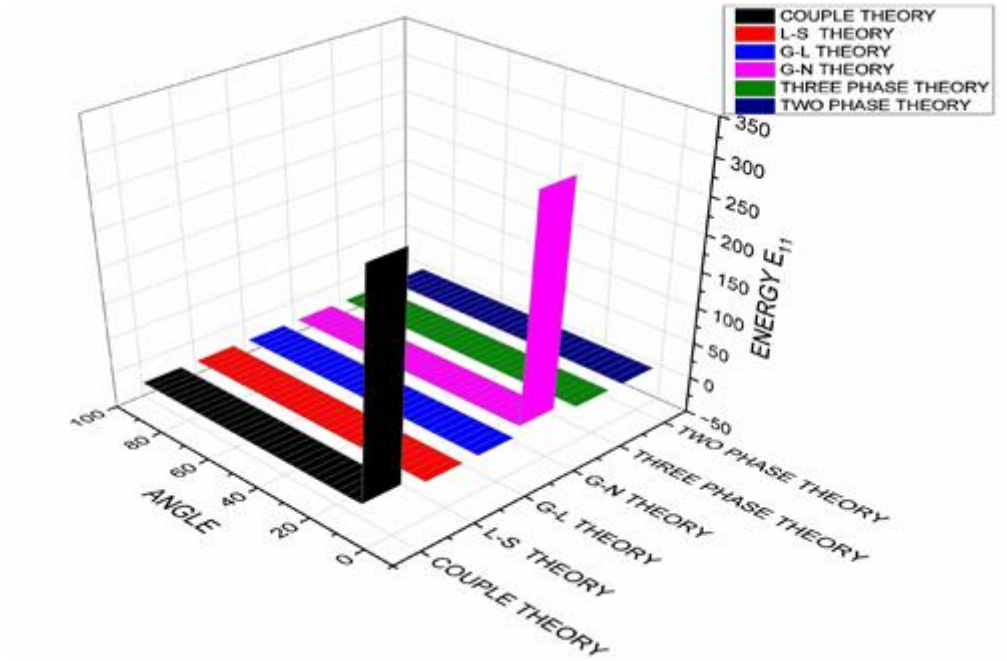

Figure 4. Changes in energy ratio E_{11} w.r.t angle $\theta°$ for P wave.

Figure 4 indicates that for L-S, G-L, the three-phase-lag model attains the minimum value of energy as the $\theta°$ increases from 0° to 90°. The coupled model and G-N model attain maximum value, decrease continuously, and then attain minimum value in the range $18° \leq \theta° \leq 90°$. The two-phase-lag model attains a comparatively higher value than L-S, G-L and the three-phase-lag model, but there is not much difference as the $\theta°$ increases from 0° to 90°.

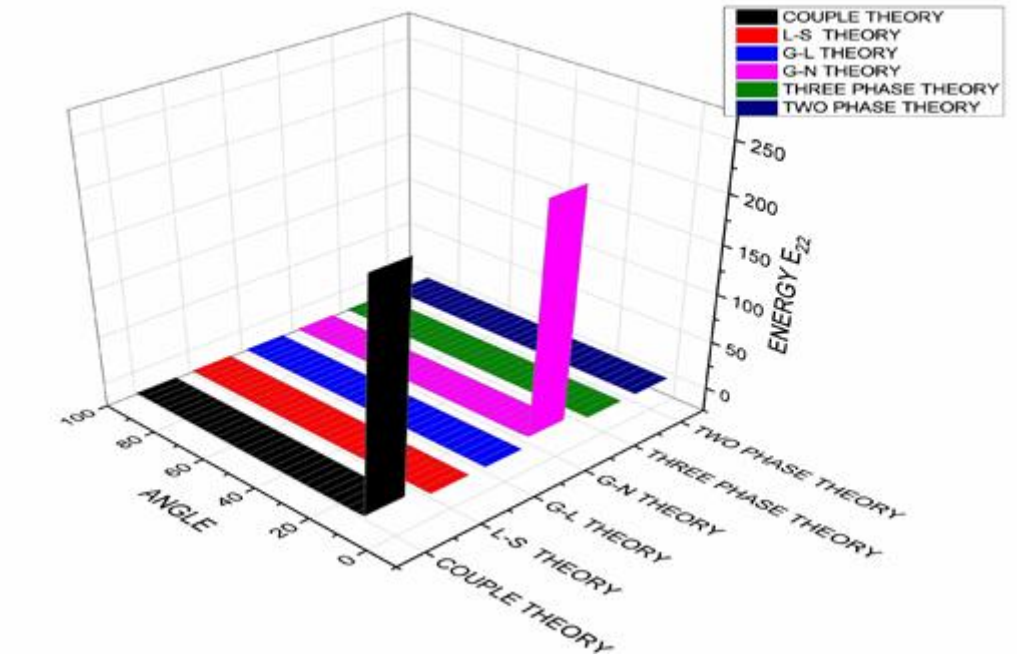

Figure 5. Changes in energy ratio E_{22} w.r.t angle $\theta°$ for P wave.

Figure 5 shows that E_{22} has the same behavior and changes as in E_{11}, but the magnitude values are different. For L-S, G-L, two-phase-lag and three-phase-lag

model attain the minimum value of energy as the $\theta°$ increases from 0° to 90°. The coupled model and G-N model attain maximum value at $\theta°$ = 17°, after which it decreases continuously and then attains minimum value in the range $18° \leq \theta° \leq 90°$. The two-phase-lag model attains a comparatively higher value than L-S, G-L and the three-phase-lag model, but there is not much difference as the $\theta°$ increases from 0° to 90°.

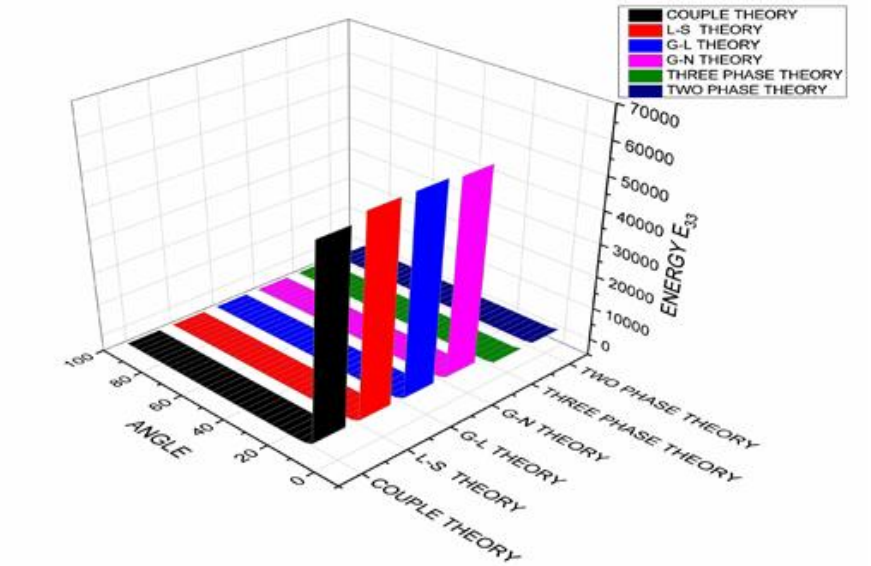

Figure 6. Changes in energy ratio E_{33} w.r.t angle $\theta°$ for P wave.

Figure 6 depicts that the two-phase-lag model and the three-phase-lag model E_{33} attain the minimum value in the range $10° \leq \theta° \leq 90°$ and the maximum value at $\theta°$ = (0.5°). In $0° \leq \theta° \leq 10°$, the value of E_{33} decreases.

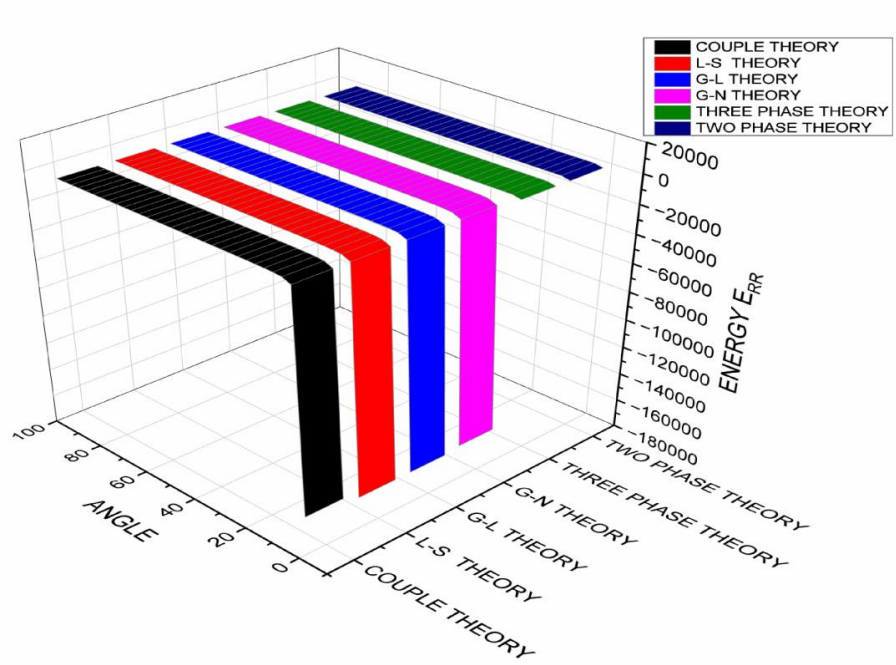

Figure 7. Changes in energy ratio E_{RR} w.r.t angle $\theta°$ for P wave.

Figure 7 depicts that for two-phase-lag and three-phase-lag models, the energy ratio E_{RR} attains a value nearly equal to zero. For coupled L-S, G-L and G-N models the value of E_{RR} attains near zero in the range $10° \leq \theta° \leq 90°$ and outside of this range energy decreases continuously until it attains its minimum value at $\theta° = 7°$.

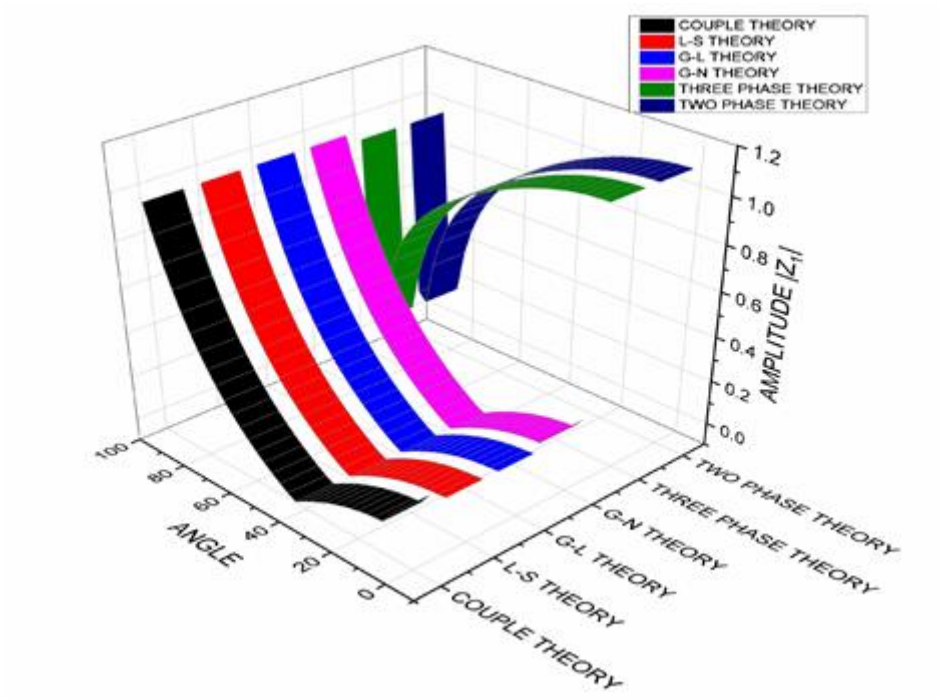

Figure 8. Changes in amplitude ratio $|Z_1|$ w.r.t angle $\theta°$ for P wave.

Figure 8 shows that the values of $|Z_1|$ decrease in the range $20° \leq \theta° \leq 40°$ and after that, they increase continuously with an increase in angle for the coupled L-S, G-N and G-L models. For two-phase-lag and three-phase-lag theories, after attaining the maximum value, the value $|Z_1|$ decreases continuously.

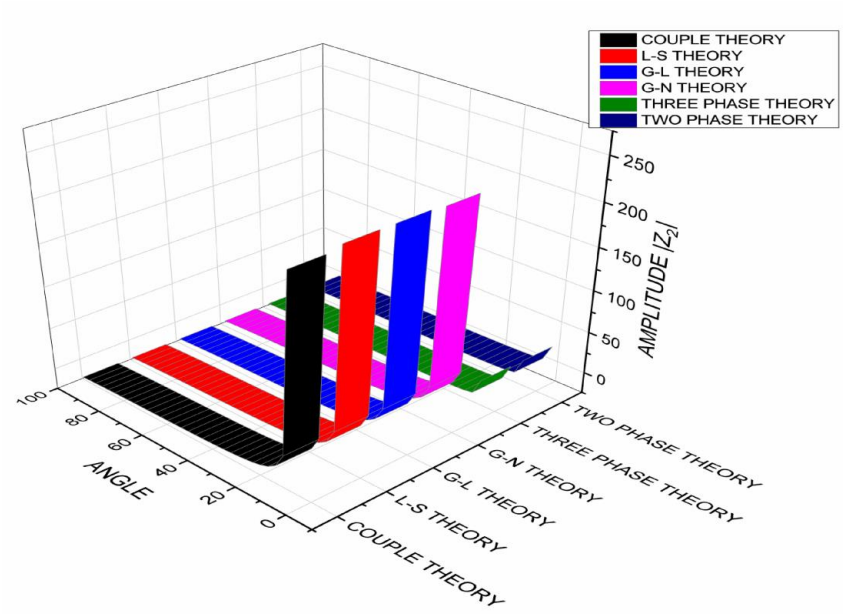

Figure 9. Changes in amplitude ratio $|Z_2|$ w.r.t angle $\theta°$ for P wave.

Figure 9 shows that for the coupled L-S, G-N and G-L models, the value of $|Z_2|$ attains the maximum value at $\theta° = 19°$ after it gives a constant value near to zero. For the other two models, three-phase-lag and two-phase-lag, it remained constant nearing zero when the angle $\theta°$ increases in the range of $0° \leq \theta° \leq 90°$, respectively.

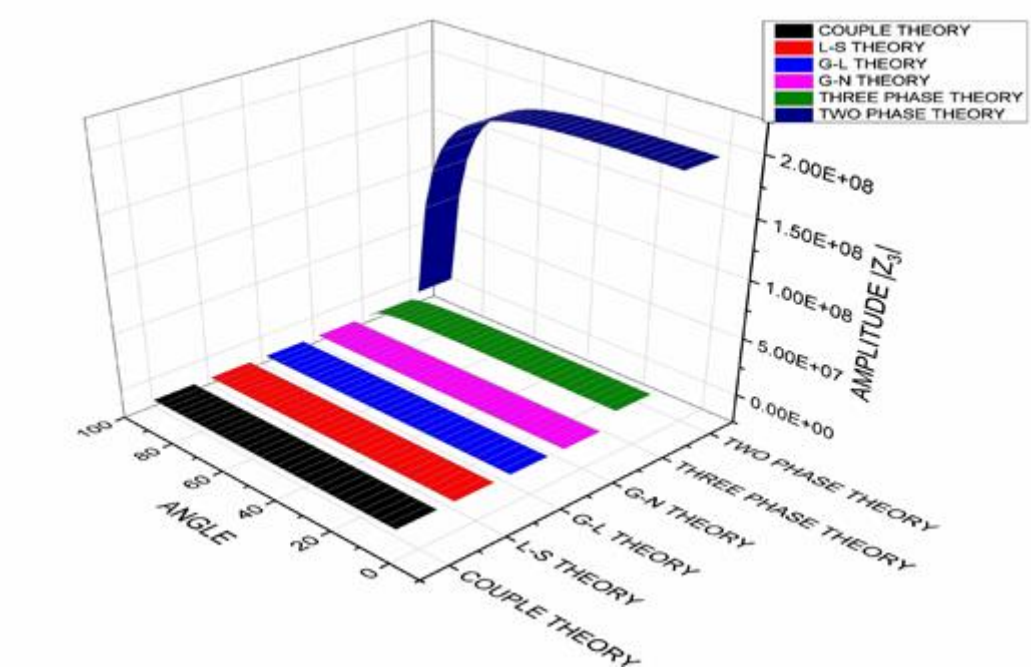

Figure 10. Changes in amplitude ratio $|Z_3|$ w.r.t angle $\theta°$ for P wave.

In **Figure 10**, the value of $|Z_3|$ depicts the same behavior and variations for all the models show values near to zero. For the two-phase-lag model, the value of the amplitude ratio decreases continuously as the $\theta°$ increases in the range $0° \leq \theta° \leq 90°$.

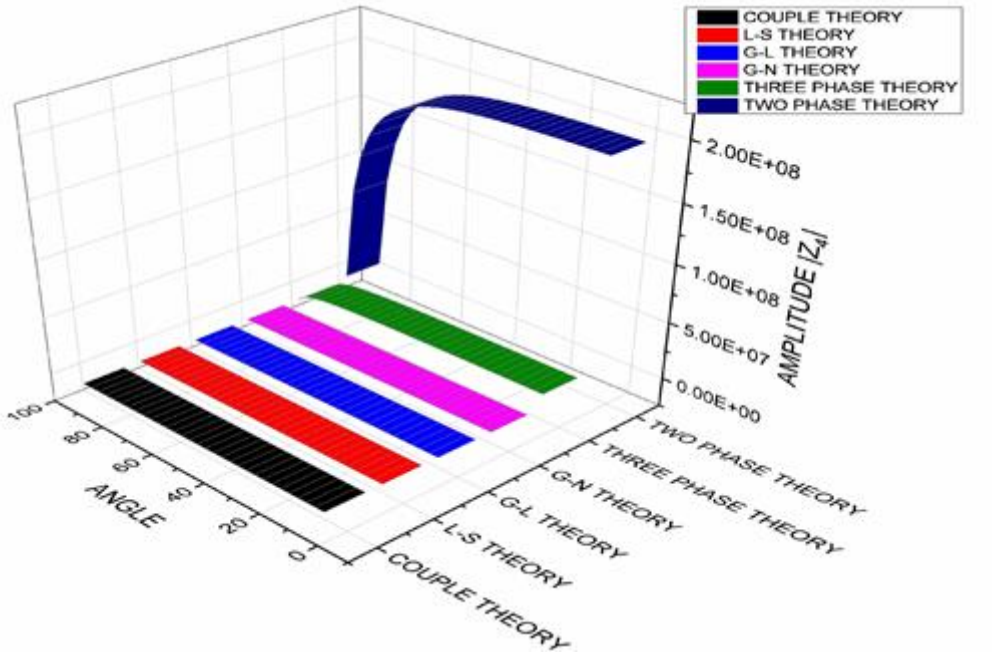

Figure 11. Changes in amplitude ratio $|Z_4|$ w.r.t angle $\theta°$ for P wave.

Figure 11. The values of $|Z_4|$ depict the same behavior and variations for all the models show values near zero for increasing values of incident angle. For the two-phase-lag model, the value of amplitude decreases continuously as $\theta°$ increases in the range of angle $0° \leq \theta° \leq 90°$.

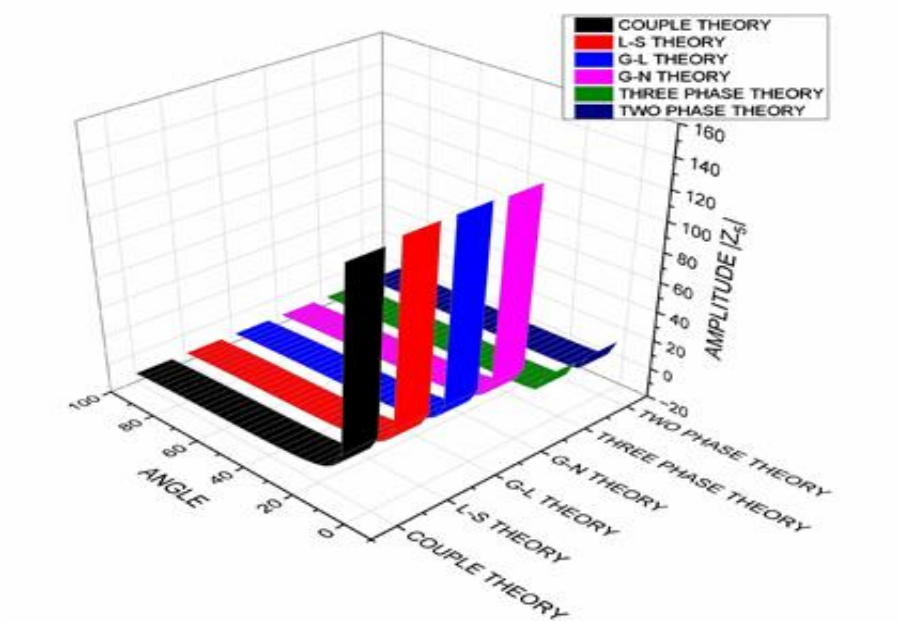

Figure 12. Changes in amplitude ratio $|Z_5|$ w.r.t angle $\theta°$ for P wave.

Figure 12 shows that for the coupled L-S, G-N and G-L models, the values of $|Z_5|$ after attaining the maximum value are constant and near zero. For the other two models, three-phase-lag and two-phase-lag, it remained constant nearing zero as $\theta°$ increases $0° \leq \theta° \leq 90°$, respectively.

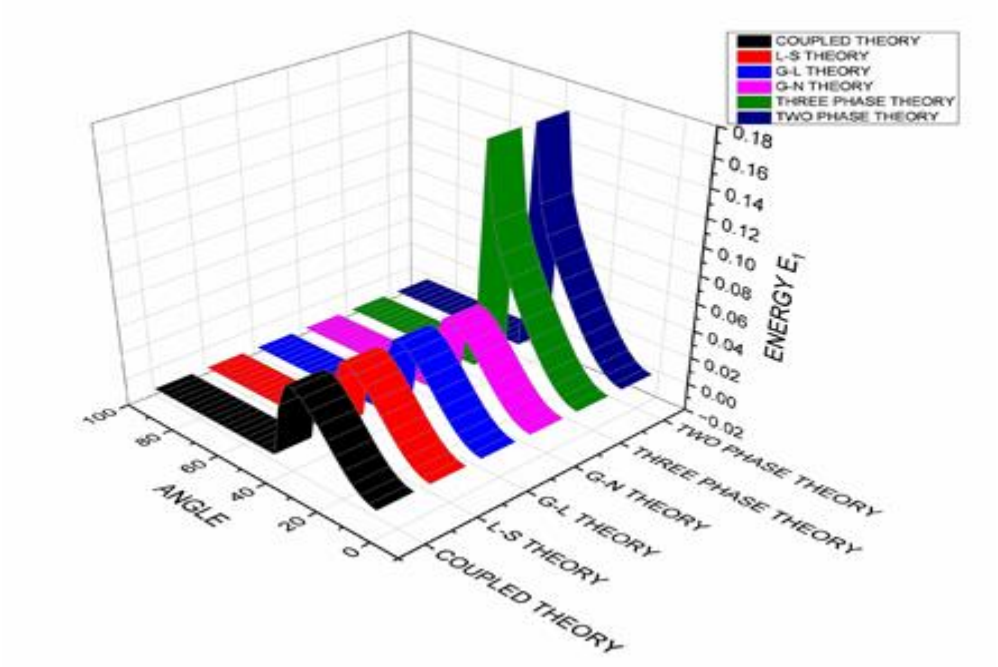

Figure 13. Changes in energy ratio E_1 w.r.t angle $\theta°$ for SV wave.

In **Figure 13**, it is concluded that all models E_1 show an increase in values as the angle increases in $0° \leq \theta° \leq 30°$, attain a maximum at $\theta° = 30°$, decrease rapidly for $30° \leq \theta° \leq 40°$ and thereafter attain a minimum value nearly at zero in the range $50° \leq \theta° \leq 90°$.

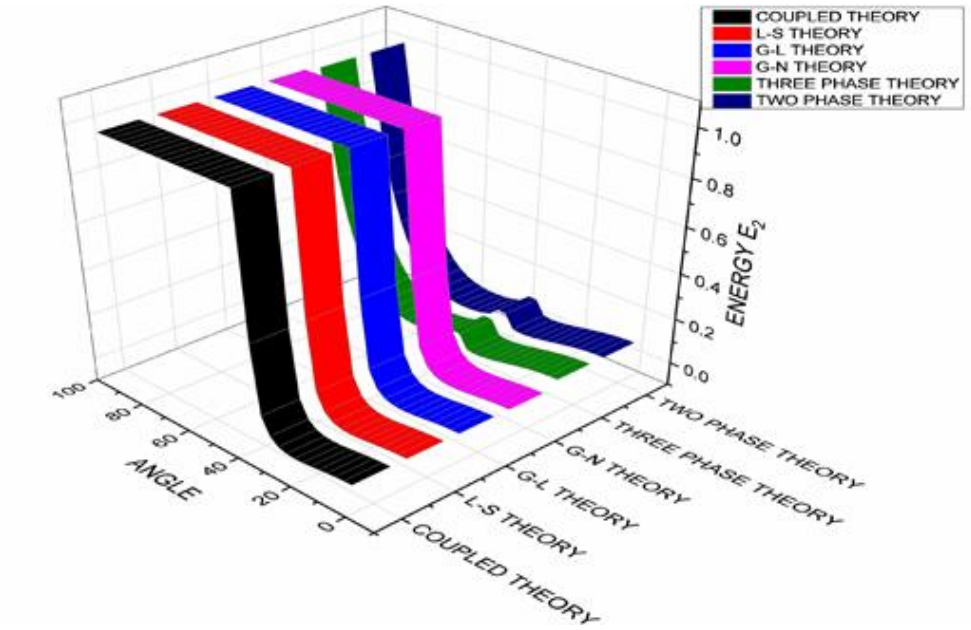

Figure 14. Changes in energy ratio E_2 w.r.t angle $\theta°$ for SV wave.

Figure 14 shows that the behavior of E_2 is opposite to E_1 and has obtained the maximum value of 1 in the interval $40° \leq \theta° \leq 90°$ for Coupled, L-S, G-L and G-N models, but the energy of two-phase-lag and three-phase-lag models increases as $\theta°$ range $40° \leq \theta° \leq 90°$ increases, reaching a maximum at $\theta° = 90°$. For $30° \leq \theta° \leq 40°$, all models show an increase in value with an increase in $\theta°$.

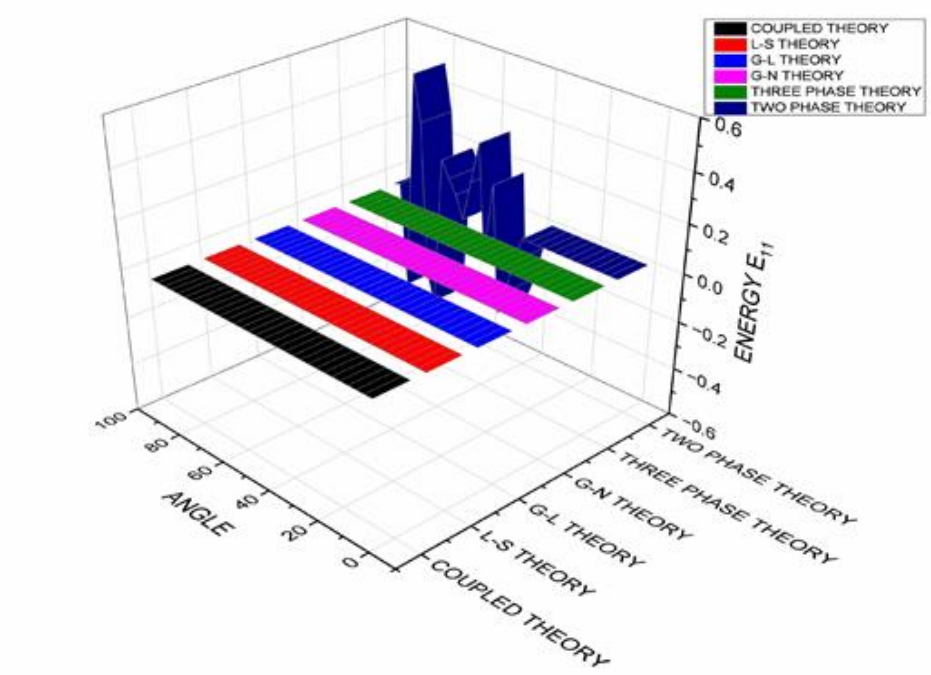

Figure 15. Changes in energy ratio E_{11} w.r.t angle $\theta°$ for SV wave.

In **Figure 15**, it is depicted that E_{11} shows similar behavior and variations for all the models coupled, L-S, G-L, G-N and the three-phase-lag except the two-phase-lag. It attains a value close to zero in the interval $0° \leq \theta° \leq 40°$ and then fluctuates for $40° \leq \theta° \leq 80°$ and finally attains a maximum value in the interval $80° \leq \theta° \leq 90°$.

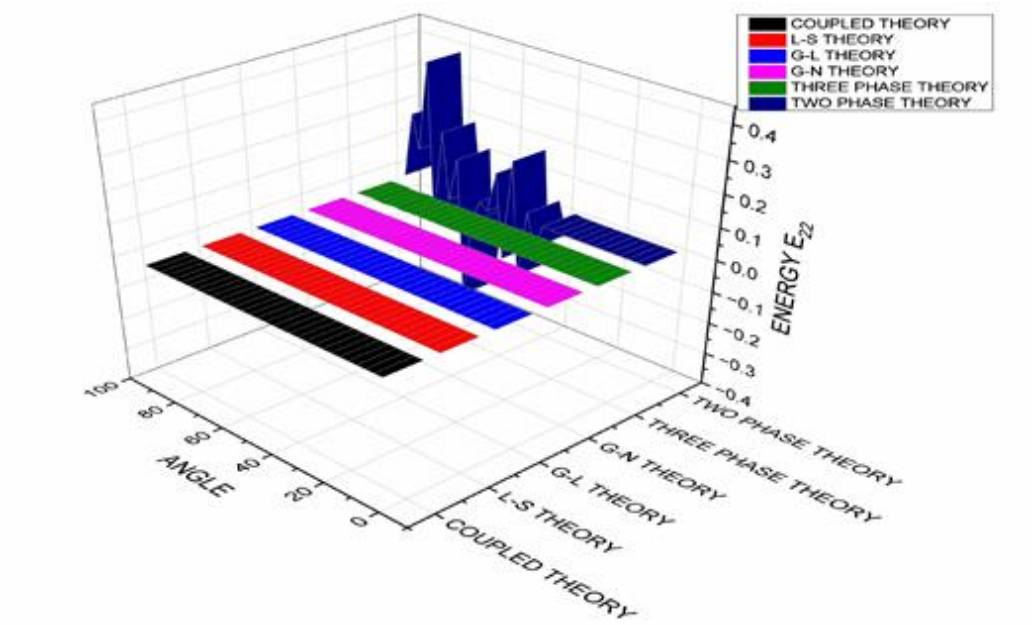

Figure 16. Changes in energy ratio E_{22} w.r.t angle $\theta°$ for SV wave.

Observation in **Figure 16** E_{22} shows similar behavior and variations for all the models except the two-phase-lag model. It attains a value close to zero in the interval $0° \leq \theta° \leq 40°$ and then fluctuates for $40° \leq \theta° \leq 80°$ and finally attains a maximum value in the interval $80° \leq \theta° \leq 90°$.

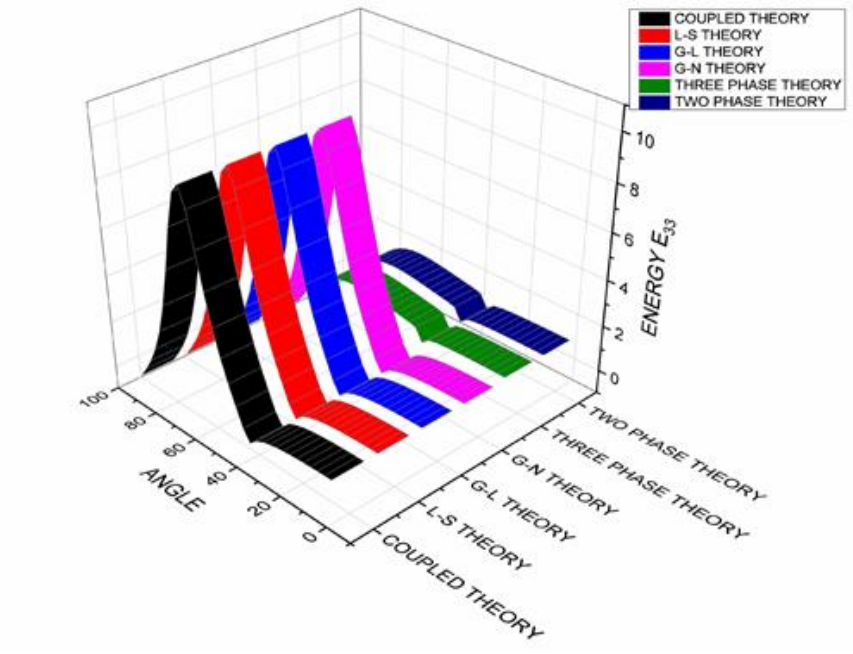

Figure 17. Changes in energy ratio E_{33} w.r.t angle $\theta°$ for SV wave.

Figure 17 indicates that E_{33} attains a value close to zero in the range $0° \leq \theta° \leq 40°$ and then fluctuates at $\theta° = 45°$. Then increases $45° \leq \theta° \leq 80°$ and attains maximum value for Couple, G-L, L-S and G-N models. After that, it decreases and attains its minimum value.

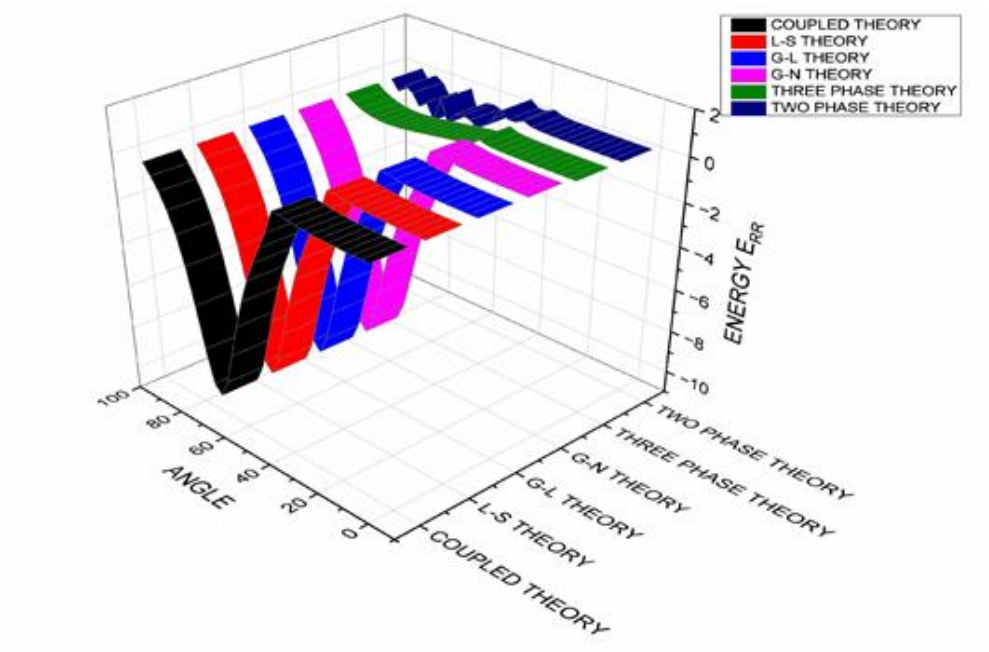

Figure 18. Changes in energy ratio E_{RR} w.r.t angle $\theta°$ for SV wave.

Figure 18 indicates that for all models, values of E_{RR} are nearly zero, decrease smoothly in the range $75° \leq \theta° \leq 80°$, attain the minimum value for $\theta° = 80°$, then increase rapidly in the range $80° \leq \theta° \leq 90°$, and finally take the value 1. But in the case of two-phase-lag and three-phase-lag model behavior, the value is near zero. Both the P and SV waves show the sum of all different energies. This holds for all the theories.

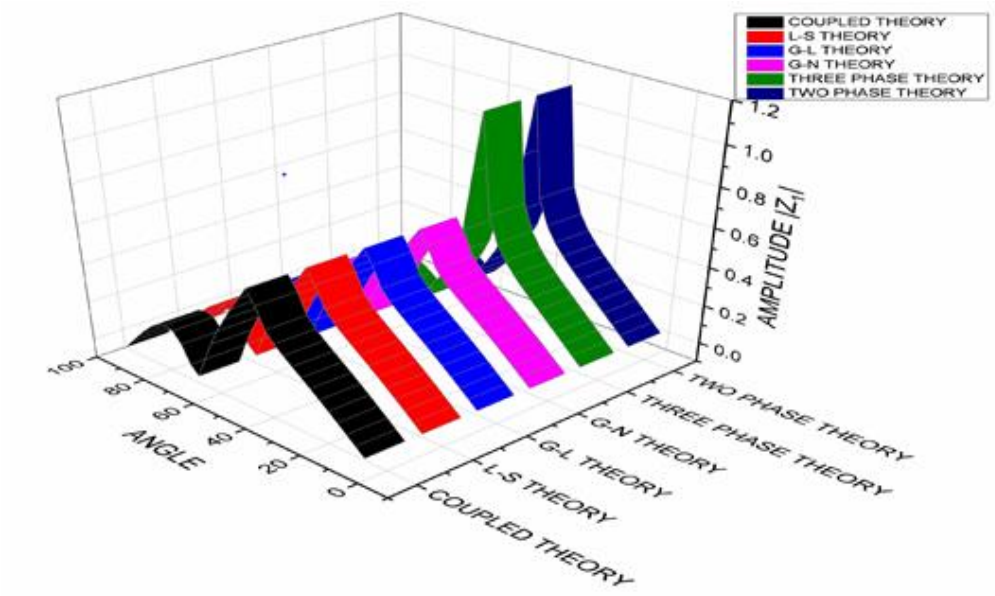

Figure 19. Changes in amplitude ratio $|Z_1|$ w.r.t angle $\theta°$ for SV wave.

From **Figure 19**, it is evident that for all models $|Z_1|$ shows an increase in values as $\theta°$ changes. It increases in the range $0° \leq \theta° \leq 50°$, attains a maximum at $\theta° = 50°$, decreases rapidly for $50° \leq \theta° \leq 75°$ and thereafter increases again after attaining a minimum value nearly to zero in the range $75° \leq \theta° \leq 85°$, then again decreases.

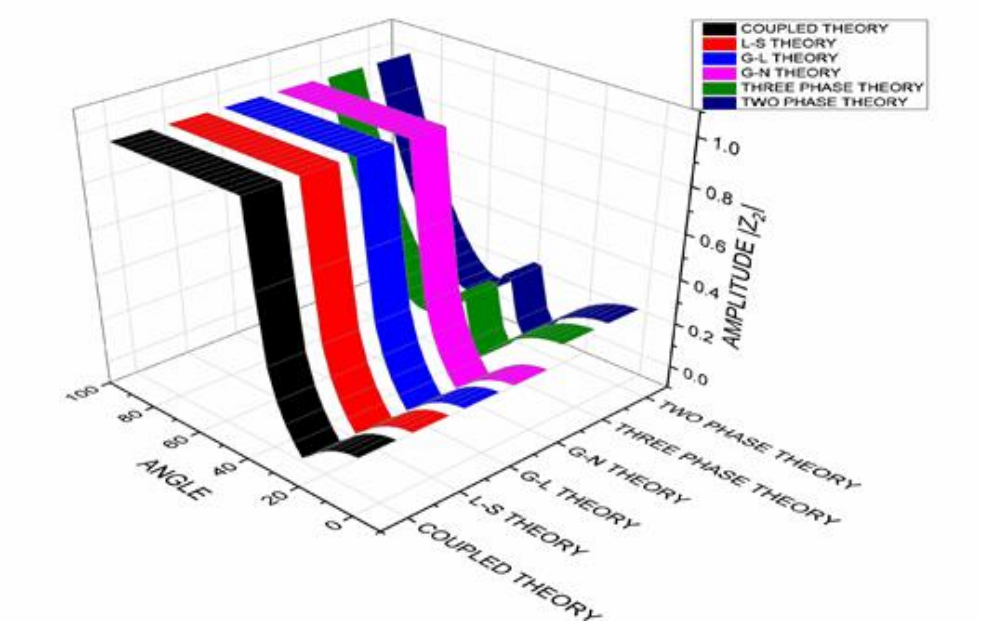

Figure 20. Changes in amplitude ratio $|Z_2|$ w.r.t angle $\theta°$ for SV wave.

Figure 20 shows that the behavior and changes of $|Z_2|$ are opposite to $|Z_1|$ and have a maximum constant amplitude value in the range $40° \leq \theta° \leq 90°$ for the Coupled, L-S, G-N and G-L models. But in two- and three-phase-lag models, fluctuating behavior is shown as $\theta°$ an increase in the range $20° \leq \theta° \leq 90°$.

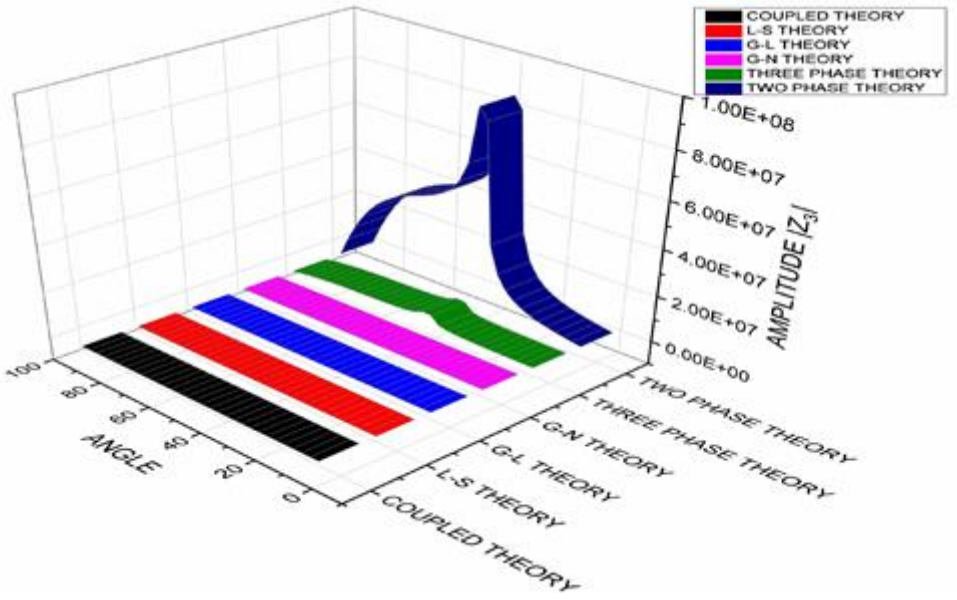

Figure 21. Changes in amplitude ratio $|Z_3|$ w.r.t angle $\theta°$ for SV wave.

In **Figure 21**, it appears that $|Z_3|$ has the same behavior and variations for Coupled, L-S, G-N, G-L and three-phase-lag models. But in the two-phase-lag model, amplitude ratio increases in the interval $0° \leq \theta° \leq 40°$ and then decreases in $40° \leq \theta° \leq 90°$.

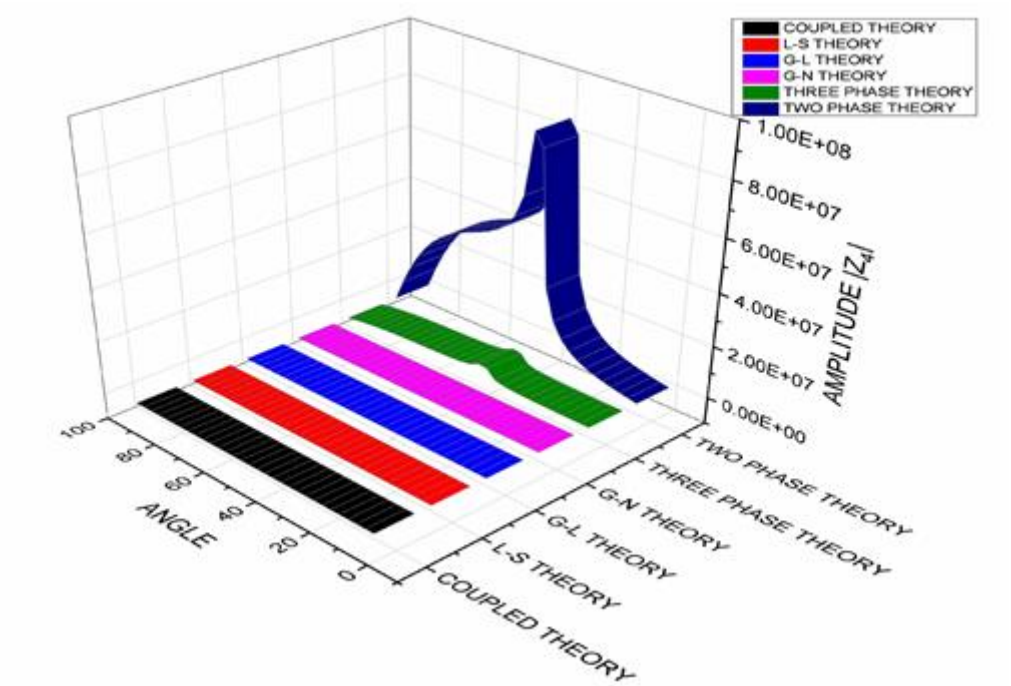

Figure 22. Changes in amplitude ratio $|Z_4|$ w.r.t angle $\theta°$ for SV wave.

In **Figure 22**, it appears that $|Z_4|$ has the same behavior and variations for all the models. In the two-phase-lag model, amplitude ratio increases in the interval $0° \leq \theta° \leq 40°$ and then decreases in $40° \leq \theta° \leq 90°$.

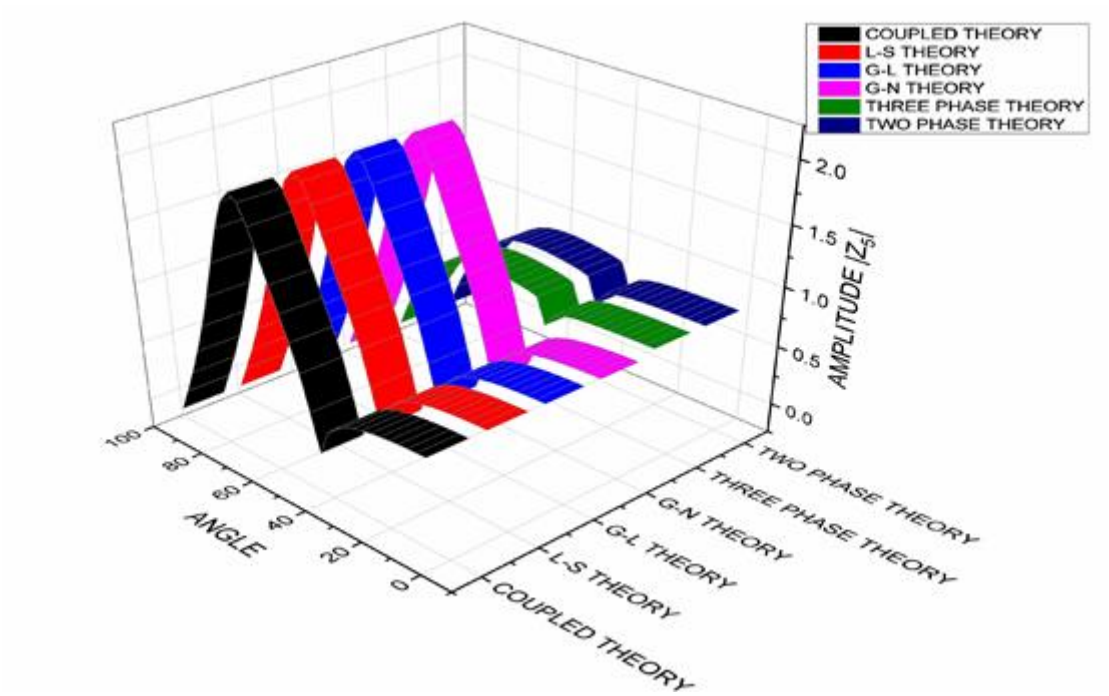

Figure 23. Changes in amplitude ratio $|Z_5|$ w.r.t angle $\theta°$ for SV wave.

From **Figure 23**, it is noticed that in the range $40° \leq \theta° \leq 60°$, amplitude $|Z_5|$ shows a constant value for all models. At $\theta° = 60°$, it attained a minimum value and then again increases as angle increases, and $85° \leq \theta° \leq 90°$ rapidly decreases.

8. Conclusion

In the current article, the phenomenon of incident elastic waves on the surface $x_3 = 0$ is discussed. Transmission and reflection at the plane between a half-space of elastic solids $x_3 < 0$ and six models in another half-space $x_3 > 0$ of thermoelastic solids (Coupled, L-S, G-N, three-phase-lag, two-phase-lag and G-L theories) has been investigated for isotropic material. Various wave conditions regarding displacement potentials are used to identify and describe the three waves in thermoelastic solid media with different models. With regard to the angle of incidence, the proportions of energies for various refracted and reflected waves with respect to the incident wave are calculated computationally, shown visually and then compared for all six models.

Findings: The analysis of the results permits some concluding remarks:

1) All distributions show a considerable influence from the phase lag effect, which can be seen. The difference between all the thermoelastic models and dual-phase-lag (DPL) thermoelastic model is very clear.
2) Due to differences in phase lags in different thermoelastic models. Differences in energy ratios and amplitude ratios are observed.
3) Graphically, it is observed that values of energy for different angles in P waves achieve the highest and lowest values as compared to SV waves. But still, both acquired the sum of energies as one.
4) We draw the conclusion from numerical results that for all theories of the thermoelastic model, the influence of the angle of incidence on amplitude and energy ratio is substantial.
5) The law of incident energy conservation at the interface is guaranteed by the fact that the total energy ratio of all reflected waves, refracted waves and involvement between refracted waves reliably ends up being unity. It is noticed that the sum of the values of E_1, E_2, E_{11}, E_{33}, E_{22} and E_{RR} energy ratios is found to be unity at each value $\theta°$, which proves the law of conservation of energy in the medium considered.
6) The considered problem has applications in astronautics, earthquake engineering, rocket engineering, and many more engineering areas.

Author contributions: Conceptualization, KK, VG and SG; methodology, KK, VG and SG; software, SG and MK; validation, KK, VG and SG; formal analysis, KK, VG, SG and MK; investigation, KK, VG and SG; data curation, KK, VG and SG; writing—original draft preparation, SG; writing—review and editing, KK, VG and SG; supervision, KK and VG. All authors have read and agreed to the published version of the manuscript.

Conflict of interest: The authors declare no conflict of interest.

References

1. McCarthy MF. Wave propagation in generalized thermoelasticity. International Journal of Engineering Science. 1972; 10(7): 593–602.
2. Sharma JN, Sidhu RS. On the propagation of plane harmonic waves in Anisotropic generalized thermoelasticity. International Journal of Engineering Science. 1986; 24(9): 1511–1516.
3. Banerjee DK, Pao YH. Thermoelastic waves in anisotropic solids. The Journal of the Acoustical Society of America. 1974; 56(5): 1444–1454. doi: 10.1121/1.1903463
4. Puri P. Plane waves in generalized thermoelasticity. International Journal of Engineering Science. 1973; 11(7): 735–744.
5. Chadwick P, Seet LTC. Wave propagation in a transversely isotropic heat-conducting elastic material. Mathematika. 1970; 17(2): 255–274. doi: 10.1112/s002557930000293x
6. Dhaliwal RS, Sherief HH. Generalized thermoelasticity for anisotropic media. Quarterly of Applied Mathematics. 1980; 38(1): 1–8. doi: 10.1090/qam/575828
7. Chandrasekharaiah DS. Wave propagation in a thermoelastic half-space. Indian Journal of Pure and Applied Math. 1981; 12: 226–241.
8. Singh H, Sharma JN. Generalized thermoelastic waves in transversely isotropic media. The Journal of the Acoustical Society of America. 1985; 77(3): 1046–1053. doi: 10.1121/1.392391
9. Sharma MD. Wave Propagation in Anisotropic Generalized Thermoelastic Media. Journal of Thermal Stresses. 2006; 29(7): 629–642. doi: 10.1080/01495730500499100
10. Prasad R, Kumar R, Mukhopadhyay S. Propagation of harmonic plane waves under thermoelasticity with dual-phase-lags. International Journal of Engineering Science. 2010; 48(12): 2028–2043. doi: 10.1016/j.ijengsci.2010.04.011
11. Lykotrafitis G, Georgiadis HG, Brock LM. Three-dimensional thermoelastic wave motions in a half-space under the action of a buried source. International Journal of Solids and Structures. 2001; 38(28–29): 4857–4878.
12. Sharma MD. Wave propagation in a general anisotropic poroelastic medium with anisotropic permeability: phase velocity and attenuation. International Journal of Solids and Structures. 2004; 41(16–17): 4587–4597. doi: 10.1016/j.ijsolstr.2004.02.066
13. Venkatesan M, Ponnusamy P. Wave propagation in a generalized thermoelastic solid cylinder of arbitrary cross-section immersed in a fluid. International Journal of Mechanical Sciences. 2007; 49(6): 741–751. doi: 10.1016/j.ijmecsci.2006.10.003
14. Kumar R, Kansal T. Propagation of Lamb waves in transversely isotropic thermoelastic diffusive plate. International Journal of Solids and Structures. 2008; 45(22–23): 5890–5913. doi: 10.1016/j.ijsolstr.2008.07.005
15. Yu J, Wu B, He C. Guided thermoelastic wave propagation in layered plates without energy dissipation. Acta Mechanica Solida Sinica. 2011; 24: 135–143.
16. Kumar R, Gupta V. Reflection and transmission of plane waves at the interface of an elastic half-space and a fractional order thermoelastic half-space. Archive of Applied Mechanics. 2013; 83(8): 1109–1128. doi: 10.1007/s00419-013-0737-6
17. Youssef HM, El-Bary AA. Theory of hyperbolic two temperature generalized thermoelasticity. Journal of Material Physics and Mechanics. 2018; 40: 158–171.
18. Lata P, Kaur I, Singh K. Thermomechanical interactions due to time harmonic sources in a transversely isotropic magneto thermoelastic rotating solids in Lord-Shulman model. Journal of Material Physics and Mechanics. 2020; 46: 7–26.
19. Kumar R, Bansal P, Gupta V. Reflection and transmission at the interface of an elastic and two-temperature generalized thermoelastic half-space with fractional order derivative. Journal of Material Physics and Mechanics. 2021; 47: 1–19.
20. Sherief H, Anwar MN, El-Latief AA, et al. A fully coupled system of generalized thermoelastic theory for semiconductor medium. Scientific Reports. 2024; 14(1). doi: 10.1038/s41598-024-63554-2
21. Ding W, Patnaik S, Sidhardh S, Semperlotti F. Displacement-driven approach to nonlocal elasticity. Nanomechanics of Structures and Materials. 2024; 277–317. doi: 10.1016/b978-0-443-21949-8.00016-4
22. Li S, Zheng W, Li L. Spatiotemporally nonlocal homogenization method for viscoelastic porous metamaterial structures. International Journal of Mechanical Sciences. 2024; 282: 109572. doi: 10.1016/j.ijmecsci.2024.109572
23. Kumar R, Kaushal S, Kochar A. Analysis of axisymmetric deformation in generalized micropolar thermoelasticity within the framework of Moore-Gibson-Thompson heat equation incorporating non-local and hyperbolic two-temperature effect. The Journal of Strain Analysis for Engineering Design. 2024; 59(3): 153–166. doi: 10.1177/03093247241232180

24. Yadav AK, Carrera E, Marin M, Othman MIA. Reflection of hygrothermal waves in a Nonlocal Theory of coupled thermo-elasticity. Mechanics of Advanced Materials and Structures. 2024; 31(5): 1083–1096. doi: 10.1080/15376494.2022.2130484
25. Abd-Alla AM, Othman MIA, Abo-Dahab SM. Reflection of Plane Waves from Electro-magneto-thermoelastic Half-space with a Dual-Phase-Lag Model. Computers Materials & Continua. 2016; 51(2): 63–79.
26. Othman MIA, Abo-Dahab SM, Alsebaey ONS. Reflection of Plane Waves from a Rotating Magneto-thermoelastic Medium with Two-temperature and Initial Stress under Three Theories. Mechanics and Mechanical Engineering. 2017; 21(2): 217–232.
27. Biot MA. Thermoelasticity and Irreversible Thermodynamics. Journal of Applied Physics. 1956; 27(3): 240–253. doi: 10.1063/1.1722351
28. Lord HW, Shulman Y. A generalized dynamical theory of thermo-elasticity. Journal of Mechanics and Physics of Solids. 1967; 15(5): 299–309.
29. Green AE, Lindsay KA. Thermoelasticity. Journal of Elasticity. 1972; 2(1): 1–7. doi: 10.1007/bf00045689
30. Green AE, Naghdi PM. On undamped heat waves in an elastic solid. Journal of Thermal Stresses. 1992; 15(2): 253–264. doi: 10.1080/01495739208946136
31. Green AE, Naghdi PM. Thermoelasticity without energy dissipation. Journal of Elasticity. 1993; 31(3): 189–208. doi: 10.1007/bf00044969
32. Choudhuri SKR. On a thermoelastic three-phase-lag model. Journal of Thermal Stresses. 2007; 30(3): 231–238. doi: 10.1080/01495730601130919
33. Tzou DY. A unified field approach for heat conduction from macro- to micro-scales. Journal of Heat Transfer. 1995; 117(1): 8–16. doi: 10.1115/1.2822329
34. Kumar R, Kansal T. Reflection and refraction of plane waves at the interface of an elastic solid half-space and a thermoelastic diffusive solid half-space. Archives of Mechanics. 2012; 64: 293–317.
35. Borcherdt RD. Reflection-refraction of general P-and type-I S-waves in elastic and anelastic solids. Geophysical Journal of the Royal Astronomical Society. 1982; 70(3): 621–638. doi: 10.1111/j.1365-246x.1982.tb05976.x
36. Achenbach JD. In: Wave propagation inelastic solids. Elsevier Science Publishers; 1973.
37. Sherief HH, Saleh HA. A half-space problem in the theory of generalized thermoelastic diffusion. International Journal of Solids and Structures. 2005; 42(15): 4484–4493. doi: 10.1016/j.ijsolstr.2005.01.001
38. Bullen KE. In: An introduction to the theory of seismology. Cambridge University Press; 1963.

Appendix A

$$c_{11} = -\lambda^e\left(\frac{\xi_R}{\omega}\right)^2 - \rho\alpha^{2e}\left(\frac{dV_\alpha}{\omega}\right)^2, c_{12} = 2\mu^e\frac{\xi_R}{\omega}\frac{dV_\beta}{\omega}, c_{15} = 2\mu\frac{\xi_R}{\omega}\frac{dV_3}{\omega}, c_{21} = 2\mu^e\frac{\xi_R}{\omega}\frac{dV_\alpha}{\omega}, c_{31} = \frac{\xi_R}{\omega},$$

$$c_{22} = \mu^e\left[\left(\frac{dV_\beta}{\omega}\right)^2 - \left(\frac{\xi_R}{\omega}\right)^2\right], c_{25} = \mu\left[\left(\frac{\xi_R}{\omega}\right)^2 - \left(\frac{dV_3}{\omega}\right)^2\right], c_{32} = \frac{dV_\beta}{\omega}, c_{35} = \frac{dV_3}{\omega}, c_{41} = -\frac{dV_\alpha}{\omega},$$

$$c_{42} = \frac{\xi_R}{\omega}, c_{45} = -\frac{\xi_R}{\omega}, c_{51} = c_{52} = c_{55} = 0, c_{1j} = \lambda\left(\frac{\xi_R}{\omega}\right)^2 + \mu\beta^2\left(\frac{dV_j}{\omega}\right)^2 + \gamma n_j(1 - i\omega\tau_1)\frac{T_0}{\omega^2}.$$

$$c_{1j} = \lambda\left(\frac{\xi_R}{\omega}\right)^2 + \mu\beta^2\left(\frac{dV_j}{\omega}\right)^2 + \gamma n_j(1 - i\omega\tau_1)\frac{T_0}{\omega^2}, c_{2j} = 2\mu\frac{\xi_R}{\omega}\frac{dV_j}{\omega}, c_{3j} = -\frac{\xi_R}{\omega}, c_{4j} = -\frac{dV_j}{\omega},$$

$$\frac{dV_\alpha}{\omega} = \left(\frac{1}{\alpha^2} - \left(\frac{\xi_R}{\omega}\right)^2\right)^{\frac{1}{2}} = \left(\frac{1}{\alpha^2} - \frac{\sin^2\theta_0}{{V_0}^2}\right)^{\frac{1}{2}}, c_{5j} = in_j\frac{dV_j}{\omega} + n_j\frac{h}{\omega}, j = 3,4,$$

$$\frac{dV_\beta}{\omega} = \left(\frac{1}{\beta^2} - \frac{\sin^2\theta_0}{{V_0}^2}\right)^{\frac{1}{2}}, \frac{dV_j}{\omega} = p.v.\left(\frac{1}{{V_j}^2} - \frac{\sin^2\theta_0}{{V_0}^2}\right)^{\frac{1}{2}}.$$

Here p.v. is calculated having restriction $j = 1, 2, 3$. $dV_{jI} \geq 0$ to fulfill the decay requirement in a thermal elastic medium.

Appendix B

$$\langle P_{ij}^{*}\rangle = -\frac{\omega^4}{2}\mathrm{Re}\left[\left\{2\mu\frac{dV_i}{\omega}\frac{\xi_R}{\omega}\frac{\bar{\xi}_R}{\omega}+\lambda\left(\frac{\xi_R}{\omega}\right)^2\left(\frac{d\bar{V}_j}{\omega}\right)+\rho c_0^2\left(\frac{dV_i}{\omega}\right)^2\left(\frac{d\bar{V}_j}{\omega}\right)+\frac{\gamma m_i T_0}{\omega^2}\left(\frac{d\bar{V}_j}{\omega}\right)\right\}B_i'\bar{B}_j'\right],$$

$$\langle P_{i3}^{*}\rangle = -\frac{\omega^4}{2}\mathrm{Re}\left[\left\{-2\mu\frac{dV_i}{\omega}\frac{d\bar{V}_3}{\omega}\frac{\xi_R}{\omega}+\lambda\left(\frac{\xi_R}{\omega}\right)^2\left(\frac{\bar{\xi}_R}{\omega}\right)+\rho c_0^2\left(\frac{dV_i}{\omega}\right)^2\left(\frac{\bar{\xi}_R}{\omega}\right)+\frac{\gamma m_i T_0}{\omega^2}\left(\frac{\bar{\xi}_R}{\omega}\right)\right\}B_i'\bar{B}_3'\right],$$

$$\langle P_{3j}^{*}\rangle = -\frac{\omega^4}{2}\mathrm{Re}\left[\left\{\mu\left(\left(\frac{\xi_R}{\omega}\right)^2\frac{\bar{\xi}_R}{\omega}-\frac{\bar{\xi}_R}{\omega}\left(\frac{dV_3}{\omega}\right)^2\right)-\lambda\frac{\xi_R}{\omega}\frac{dV_3}{\omega}\frac{d\bar{V}_j}{\omega}+\rho c_0^2\frac{\xi_R}{\omega}\frac{dV_3}{\omega}\frac{d\bar{V}_j}{\omega}\right\}\bar{B}_j'B_3'\right],$$

$$\langle P_{33}^{*}\rangle = -\frac{\omega^4}{2}\mathrm{Re}\left[\left\{\mu\left(\left(\frac{dV_3}{\omega}\right)^2-\left(\frac{\xi_R}{\omega}\right)^2\right)\frac{d\bar{V}_3}{\omega}-2\mu\frac{\xi_R}{\omega}\frac{\bar{\xi}_R}{\omega}\frac{dV_3}{\omega}\right\}B_3'\bar{B}_3'\right],\ i,\mathrm{j}=1,2.$$